Applied Geochemistry 211 (2026) 107130



Contents lists available at ScienceDirect

Applied Geochemistry

journal homepage: www.elsevier.com/locate/apgeochem



Hydrogeochemical and isotopic monitoring strategies for water resource sustainability: the Pordenone Plain (NE Italy)

Dino Di Renzo [a,*], Luca Pizzino [b], Goran Vižintin [c], Carmela Vaccaro [d]

[a] Institute for Environmental Protection and Research (ISPRA), Via Vitaliano Brancati 48, Rome, 00144, Italy
[b] Istituto Nazionale di Geofisica e Vulcanologia, Sezione di Roma 1, Via di Vigna Murata 605, Rome, 00143, Italy
[c] Department of Geotechnology, Mining and Environment, Faculty of Natural Sciences and Engineering, University of Ljubljana, Aškerčeva 12, Ljubljana, 1000, Slovenia
[d] University of Ferrara, Department of Environmental and Prevention Science, C.so Ercole I D'Este 32, Ferrara, 44122, Italy

ARTICLE INFO

Editorial handling by Elisa Sacchi

Keywords:
Seasonal monitoring
Hydrochemistry
Water isotopes
Groundwater management
Groundwater dynamics
Climate impact on groundwater

ABSTRACT

This study investigates the seasonal hydrogeochemical dynamics of the Pordenone Plain hydrogeological system (NE Italy). Despite abundant water resources, the system faces increasing anthropogenic and climatic stress. A hydrogeochemical conceptual model was previously developed for this setting. Building on this foundation, the present study examines the processes governing seasonal groundwater dynamics, recharge variability, and the system's response to extreme hydroclimatic events. The results reveal marked seasonal variations among aquifers, reflecting hydro-lithological differences and providing a baseline for assessing aquifer resilience to future climate-driven recharge changes. The complex and heterogeneous intermediate flow system comprises two main flow paths. The first feeds foothill karst springs, responding rapidly to pre-Alpine/Alpine precipitation and snowmelt but experiencing reduced discharge during dry periods. The second flow path recharges the alluvial plain aquifers. High and Low Plain aquifers contrast, separated by the resurgence belt, a marked permeability transition. High Plain aquifers exhibit seasonal variations closely linked to piezometric fluctuations, whereas Low Plain aquifers display an inverted seasonal pattern. This inversion reflects the permeability contrast along the resurgence belt, which is inferred to decrease groundwater flow velocities and induce a "delayed seasonal recharge response". Conversely, the deep flow system remains unaffected by surface variations, indicating that deep confined aquifers are effectively decoupled from shallow hydrogeological dynamics. This integrated geochemical and isotopic approach enables the characterization of aquifer vulnerability and seasonal recharge dynamics. When integrated with quantitative hydrological assessments, these findings support the development of comprehensive management strategies to prevent water quality degradation and promote long-term groundwater sustainability.

1. Introduction

The availability and stability of water resources play a fundamental role in ensuring food security, managing pollution in rural and urban areas, supporting energy production, fostering industrial development, and sustaining economic growth. These resources are increasingly at risk, not only from direct human activities such as agricultural and industrial pollution, but also from the broader impacts of long-term climatic trends and increasing hydroclimatic variability. The (IPCC, 2021) emphasizes that climate change significantly alters the water cycle, increasing hydrological variability and posing serious risks to the long-term sustainability of water, food, and energy systems (Oki and Kanae, 2006; Jiménez Cisneros et al., 2014; Schewe et al., 2014; Mekonnen and Hoekstra, 2016; Egidio et al., 2024).

The growing demand for groundwater for agriculture, industry, and domestic use, combined with the pressures associated with changing hydroclimatic conditions, underscores the urgent need for effective groundwater protection and management (EEA, 2018; Obergfell et al., 2019; Witte et al., 2019; Naranjo-Fernández et al., 2020; Jasechko et al., 2024). The sustainable management of groundwater is important, not only to secure drinking water, but also to support safe agriculture and to meet the needs of human activities while preventing conflicts over limited resources (Krueger et al., 2019; Mercure et al., 2019). To avoid overexploitation of this resource, understanding how

* Corresponding author. -
E-mail address: dino.direnzo@isprambiente.it (D. Di Renzo).

https://doi.org/10.1016/j.apgeochem.2026.107130
Received 2 February 2026; Received in revised form 20 October 2026; Accepted 20 October 2026
Available online 21 October 2026
0883-2927/© 2026 Elsevier Ltd. All rights are reserved, including those for text and data mining, AI training, and similar technologies.

aquifers respond to both natural and anthropogenic pressures is essential for developing robust, science-based management strategies. However, conducting groundwater studies remains challenging. Common limitations include data gaps, poor data quality, and insufficient conceptual models to explain system behaviour (e.g. Terasmaa et al., 2020). Specifically, in complex alluvial systems, conventional approaches often rely on spatial snapshots that may mask high-resolution seasonal variability and the nonlinear response of multi-aquifer domains to extreme hydroclimatic events (Ansari et al., 2023, 2025). As climate change increases the frequency of prolonged droughts and alters precipitation patterns, understanding seasonal geochemical and isotopic variability becomes a critical prerequisite for sustainable water resource management (Kumar and Ansari, 2021; Noble and Ansari, 2019). Establishing a robust seasonal baseline is central to distinguishing natural hydroclimatic fluctuations from anthropogenic pressures, detecting early signs of water quality degradation, and evaluating the capacity of aquifers to recover under stress. From this perspective, assessing seasonal hydrogeochemical variations in a hydrogeological system at the catchment scale provides a clearer picture of how aquifers evolve over time and helps identify both hydroclimatic and anthropogenic stressors (Ciampittiello et al., 2024). When integrated with quantitative hydrological data, these insights provide the hydrogeochemical baseline required to support the design and implementation of sustainable groundwater management practices.

The Friuli-Venezia Giulia region in north-eastern Italy possesses high-quality freshwater resources that support domestic, agricultural, and industrial activities. A slightly positive water balance has been documented at the regional level (Zini et al., 2011). Despite this, the region is experiencing growing pressure on groundwater resources, particularly during dry seasons. Changing rainfall and snowmelt patterns, combined with increased water use for irrigation and domestic purposes, are contributing to this pressure. Observable consequences include the progressive contraction of the resurgence belt (Zini et al., 2011), a lowering of groundwater levels in the phreatic aquifers of the High Plain (HP; Cucchi et al., 1999; Calligaris et al., 2010; Zini et al., 2013), and reduced pressures in the confined aquifers of the Low Plain (LP; Cucchi et al., 1999; Martelli and Granati, 2007; Martelli et al., 2007). These effects are especially evident during the summer months as a result of changes in rainfall patterns and increased groundwater withdrawals (Di Renzo et al., 2023).

Within this regional context, the aim of this study is to conduct a comprehensive seasonal geochemical and isotopic monitoring programme of the complex alluvial aquifer systems in the Pordenone Plain (PP). This research aims to improve our understanding of the hydrogeochemical dynamics governing groundwater quality and its spatial and temporal evolution. A previous study of the PP (Di Renzo et al., 2024) successfully established a spatially resolved, static hydrogeochemical conceptual model; however, it primarily relied on static datasets and therefore lacked the temporal resolution needed to capture dynamic seasonal shifts. Building upon this existing hydrogeochemical conceptual model, the present study introduces a seasonal monitoring approach with relatively high temporal resolution, although covering a short monitoring period, to explore the dynamic behaviour of these aquifers, focusing on how short-term hydroclimatic variability and anthropogenic factors influence the hydrodynamics of the PP. Furthermore, by using the PP, a complex and heterogeneous alluvial system characterized by marked permeability contrasts, as a benchmark, this study proposes a methodological framework that could be applicable to other comparable hydrogeological settings. The approach developed here to distinguish seasonal anomalies from baseline conditions provides a potential framework for assessing aquifer resilience in similar complex hydrogeological settings worldwide under conditions of increasing climate variability.

Ultimately, at the local scale, this study seeks to provide critical insights into the functioning of the PP groundwater systems, establishing a robust hydrogeochemical baseline to support effective and sustainable water resource management strategies in the face of future environmental and societal challenges.

2. Geological and hydrogeological settings

The Friuli Plain (FP), located in the north-eastern sector of Italy, represents the easternmost margin of the Po Valley. This area is distinguished by its steeper slopes and coarser sediments compared with the central sectors of the Po Valley (Zini et al., 2013). It covers approximately 2900 km^2 and is bordered by the Julian and Carnic Alps to the north, the Adriatic Sea to the south, the Trieste Karst to the east, and the Venetian Plain to the west (Fig. 1a).

The current geological and hydrogeological configuration of the FP is the result of depositional processes that occurred during the Upper Pleistocene, influenced by sea-level fluctuations caused by Quaternary glacial cycles and the tectonic evolution of the region (Florineth and Schluchter, 2000; Orombelli and Ravazzi, 1996). These processes led to the accumulation of clastic materials of fluvio-glacial, marine, lagoonal, and palustrine origin. The Würmian glaciation played a key role in shaping the plain, resulting in the formation of concentric moraine arcs along the main rivers. Sedimentary deposits display an N-S decrease in grain size, reflecting changes in fluvial transport and depositional dynamics (Fontana, 2006). As described by Teatini et al. (2015), the spatial variability in sediment grain size defines two main sectors of the plain.

- HP, dominated by gravel deposits interspersed with cemented sands and clay layers. These sediments, derived from the erosion of Mesozoic calcareous and dolomitic rocks (Martelli and Granati, 2007, 2010; Zini et al., 2013), were rapidly deposited during the progradation of fluvial megafans at the Last Glacial Maximum in the Upper Pleistocene (Fontana, 2006, Fontana et al., 2008). The HP may be subdivided into two distinct sectors, the upper plain primarily consisting of gravelly sediments, and the lower plain characterized by conglomerate deposits (Di Renzo et al., 2024).
- LP, characterized by clayey deposits of low permeability, interbedded with sand and gravel layers and formed during transgressive and regressive marine phases (Martelli and Granati, 2007; Zini et al., 2011).

From a hydrogeological point of view, the FP hosts a complex aquifer system. The HP is dominated by a continuous phreatic aquifer within highly permeable gravelly and sandy deposits, recharged by direct infiltration, river seepage, and subsurface contributions from the morainic hills and the pre-Alps/Alps sectors (Stefanini, 1978; Mosetti, 1983). Moving southward, the aquifer gradually transitions into a multilayered system composed of alternating permeable and impermeable sediments, forming a series of confined and semi-confined aquifers (Mosetti, 1983; Stefanini and Cucchi, 1976, 1977; Cucchi et al., 1999). A key feature is the resurgence belt, a narrow WNW–ESE zone where groundwater discharges at the surface due to the abrupt reduction in sediment permeability (Cucchi et al., 1999).

The PP, located in the northwestern sector of the FP, spans approximately 607 km^2 and is primarily situated within the alluvial fan of the Cellina River. The hydrogeological regime of the PP is largely governed by precipitation in the surrounding mountainous watersheds, where annual rainfall ranges from 2000 to 3000 mm (ARPA-OSMER, 2008). The hydrogeological setting of the PP can be broadly divided into three main components (Fig. 1b).

- The Cansiglio-Piancavallo karst system, composed of Triassic-Miocene limestones and dolomites, hosting a significant carbonate aquifer (Cavallin, 1979; Filippini et al., 2018). This karst aquifer supplies major springs at the eastern foot of the plateau, with average annual discharges ranging between 2.5×10^8 and 3.5×10^8 m^3/year (Meneghel et al., 1986; Filippini et al., 2018).

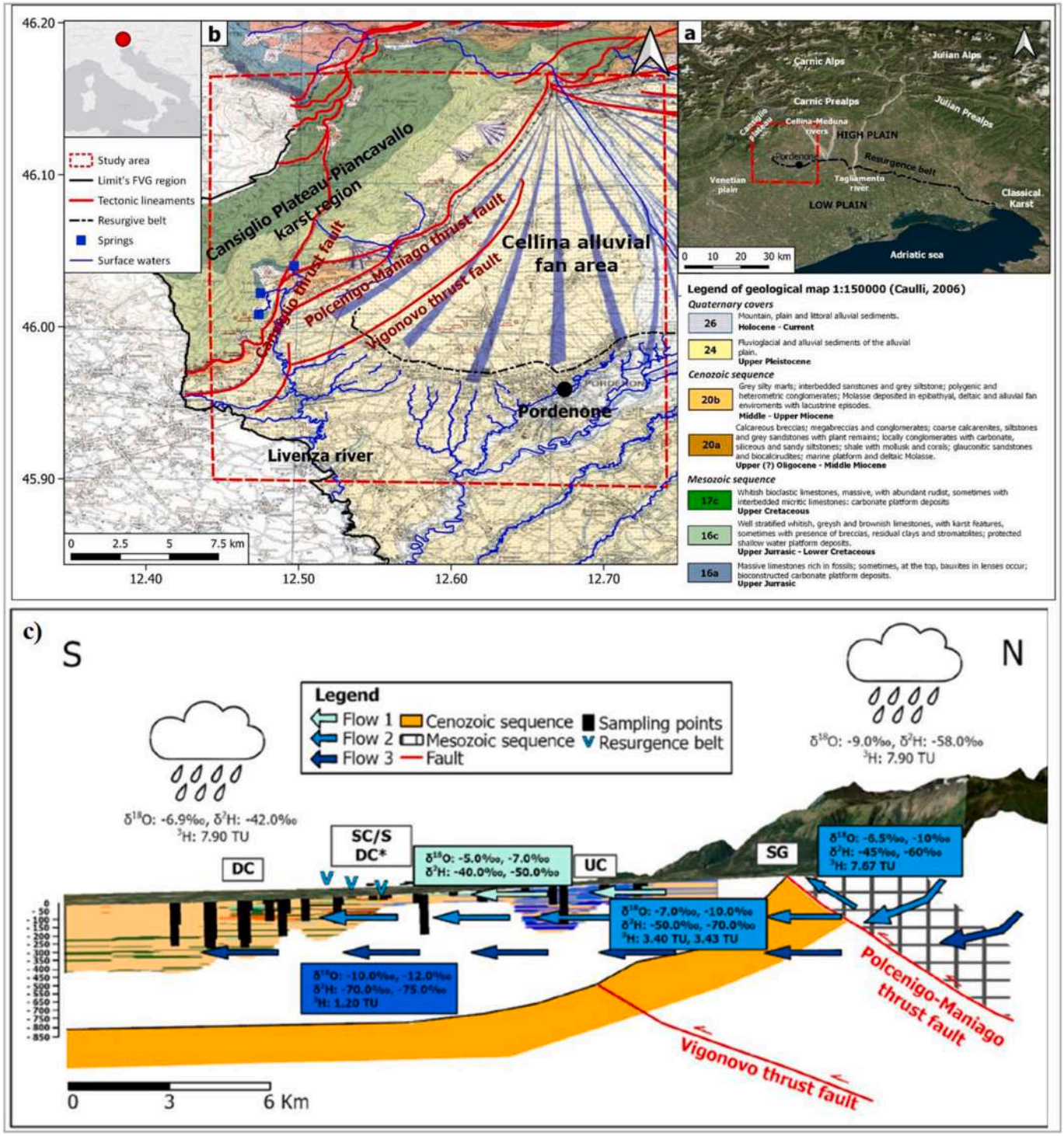


Fig. 1. Map of the study area: a) simplified map of the Friuli plain; b) geological map of the Pordenone Plain (PP) modified from Carulli (2006). The main tectonic lineaments (the Cansiglio thrust fault, Polcenigo-Maniago thrust system and Vigonovo thrust fault), the karst springs and the surface water are visible on the map. c) Conceptual hydrogeochemical model of the PP by Di Renzo et al. (2024). "DC" – depth confined aquifers; "SC/S" – semi-confined/shallow aquifers; "UC" – unconfined aquifers; "SG" – spring waters. Figure from Di Renzo et al. (2024).

- The alluvial deposits of the Cellina and Meduna Rivers, characteristic of the HP, containing an undifferentiated phreatic aquifer with high permeability (from 10^{-2} to 7×10^{-3} m/s; Cucchi et al., 2008). The HP aquifer is primarily recharged by river infiltration and direct precipitation, with an estimated annual contribution of approximately 9.6×10^{8} m^3/year. An additional average annual recharge of about 9.2×10^{8} m^3/yr occurs directly in the plain, primarily due to effective infiltration and irrigation return flow (Zini et al., 2011).
- The LP deposits, south of the resurgence belt, comprising a confined or semi-confined multilayered aquifer system with lower permeability (from 2.5×10^{-4} to 5×10^{-5} m/s; Zini et al., 2011; Cucchi et al., 2008). The HP aquifer provides recharge to both the resurgence belt and the aquifer systems of the LP, with an average total

contribution of about 1.9 × 10^9 m^3/yr. Of this recharge, approximately 1.5 × 10^9 m^3/yr is drained by the resurgence belt, while about 3.9 × 10^8 m^3/yr contributes to the confined multi-layer aquifer system of the LP (Zini et al., 2011).

However, these recharge inputs are significantly affected not only by changing hydrodynamic conditions but also by intensive groundwater abstraction for agricultural, industrial, and domestic purposes. In some cases, abstraction rates exceed natural recharge, aggravating the already negative water balance in both the HP and LP aquifers. For a detailed analysis of the hydrogeological balance, see Zini et al. (2011) and Di Renzo et al. (2024).

2.1. Hydrogeochemical model of Pordenone Plain

The conceptual hydrogeochemical model of the PP, developed by Di Renzo et al. (2024), provides a detailed framework for understanding the distinct groundwater flow systems within the study area. Illustrated in Fig. 1c, this model was established through a multidisciplinary approach, combining geochemical and isotopic analyses to identify distinct flow pathways.

The study identified three main groundwater flows within of the PP area.

i) Flow 1 involves the shallower unconfined and semi-confined aquifers hosted in the gravelly sediments of the HP. The groundwater exhibits a Ca(Mg)–HCO_3 composition, primarily resulting from interactions with carbonate rocks. Although the main recharge originates from the pre-Alpine sector and primarily occurs through riverbed infiltration, it is substantially modified by local meteoric infiltration, leading to considerable mixing of recharge sources. Moreover, due to the shallow depth of these aquifers, the system is highly influenced by intensive agricultural activity, particularly through irrigation return flow.
ii) Flow 2 involves karst spring waters, unconfined aquifers within the conglomeratic deposits of the deeper HP, and the shallower semi-confined aquifers of the LP near the resurgence belt. Isotopic data confirm a rapid recharge process and short residence times, with the recharge area located in the Carnian pre-Alps (CPA) sector. A portion of this flow contributes to the Cansiglio Plateau karst system, where regional fault structures facilitate the emergence of Ca–HCO_3-type springs characterized by quick responses to recharge events (hereafter referred to as Path 1 of Flow 2). The remaining portion flows southward, initially feeding the unconfined aquifers of the HP, and subsequently recharging the semi-confined aquifers of the LP. Interaction with dolomite-rich sediments results in Mg^{2+} enrichment, modifying the water composition toward a Ca(Mg)–HCO_3-type composition (hereafter referred to as Path 2 of Flow 2).
iii) Flow 3 represents the deeper hydrogeological system within the PP, supplying the deep confined aquifers of the multilayer system in the LP. This flow originates from a recharge area located in the Carnian Alps and is characterized by low hydraulic gradients and older groundwater, indicative of prolonged residence times in the subsurface. The waters are hosted within permeable sandy lenses confined by clay layers and display a Na–HCO_3 composition, primarily resulting from extensive silicate weathering and associated ion exchange processes. The consistent geochemical and isotopic signatures suggest hydrological isolation from the other flows and minimal influence from recent recharge.

For comprehensive details, refer to Di Renzo et al. (2024).

3. Materials and methods

3.1. Hydro-meteorological characterization of the Pordenone Plain

The hydro-meteorological characterization of the PP is a significant component in understanding how climatic conditions and seasonal variability influence the geochemical and isotopic evolution of groundwater within the hydrogeological system. To achieve this, data from four meteorological stations belonging to the ARPA FVG - OSMER and GRN network were used to characterise climatic conditions and trends in the study area (http://www.meteo.fvg.it/) (Fig. 2). These stations were strategically selected to represent distinct sectors, including the LP, HP, and CPA, thereby providing broad spatial coverage of the study area. Meteorological data, including temperature and rainfall, were analysed for the period 2021-2022, enabling a detailed examination of seasonal variations. To characterise snowfall, monthly average snow-cover data from the CPA over the same period were examined to evaluate seasonal patterns of snow accumulation and their potential influence on recharge dynamics. For the hydrogeological characterization, piezometric data from four monitoring stations belonging to the groundwater monitoring network of the Hydraulic Service of the Friuli Venezia Giulia Region were analysed (Fig. 2; Table 1S). These stations, with observation records spanning over two decades, provided a robust dataset for examining piezometric trends. However, for the purpose of this research, only data recorded between January 2020 and March 2023 were considered. The analysis focused on reconstructing the temporal variations in piezometric levels within the HP aquifer during the study period. A preliminary data homogenization procedure was performed to ensure consistency among the records, followed by an analysis of piezometric trends at each monitoring station using geostatistical techniques. All hydro-meteorological data collected for this study were statistically analysed to characterise the climatic and hydrogeological conditions of the PP and assess their potential influence on groundwater dynamics.

3.2. Seasonal geochemical and isotopic monitoring of the Pordenone Plain hydrogeological system

The seasonal hydrogeochemical and isotopic monitoring of the PP was conducted between July 2021 and December 2022 through four sampling campaigns: two carried out during the summer and two during the winter. A total of 31 sampling points, including wells and karst springs, were selected to represent the two primary groundwater flows identified in a previous detailed geochemical and isotopic study: the intermediate flow (Flow 2) and the deeper flow (Flow 3). The surface flow (Flow 1) was excluded from this seasonal study due to the limited number of sampling points, which prevented a sufficiently detailed and spatially consistent characterization of seasonal variations and associated anthropogenic influences. The sampling points, previously identified in Di Renzo et al. (2024), include 3 karst springs located on the eastern slope of the Cansiglio Plateau, 12 wells distributed at different depths within the HP and the resurgence belt sectors, representing the intermediate flow system, and 16 wells in the LP representing the deeper groundwater flow (Fig. 2). The collected water samples were categorized following the same classification used in the previous study by Di Renzo et al. (2024). Non-pressurised wells were purged following international standard protocols, using low-flow methods and pumping three to four well volumes prior to sampling. Details on the well-screen depths are provided in Table 2S.

The study focused on field physicochemical measurements, major ion chemical analyses, and stable isotope analyses ($\delta^{18}O$ and $\delta^{2}H$). Field measurements for water temperature (T), pH, electrical conductivity (EC), and oxidation-reduction potential (ORP) were performed using multiparameter probes, with manufacturer-reported accuracies of ±0.1 °C for T, ±0.01 for pH, and ±1% for EC. Total alkalinity was determined by acidimetric titration with 0.05 N HCl using methyl

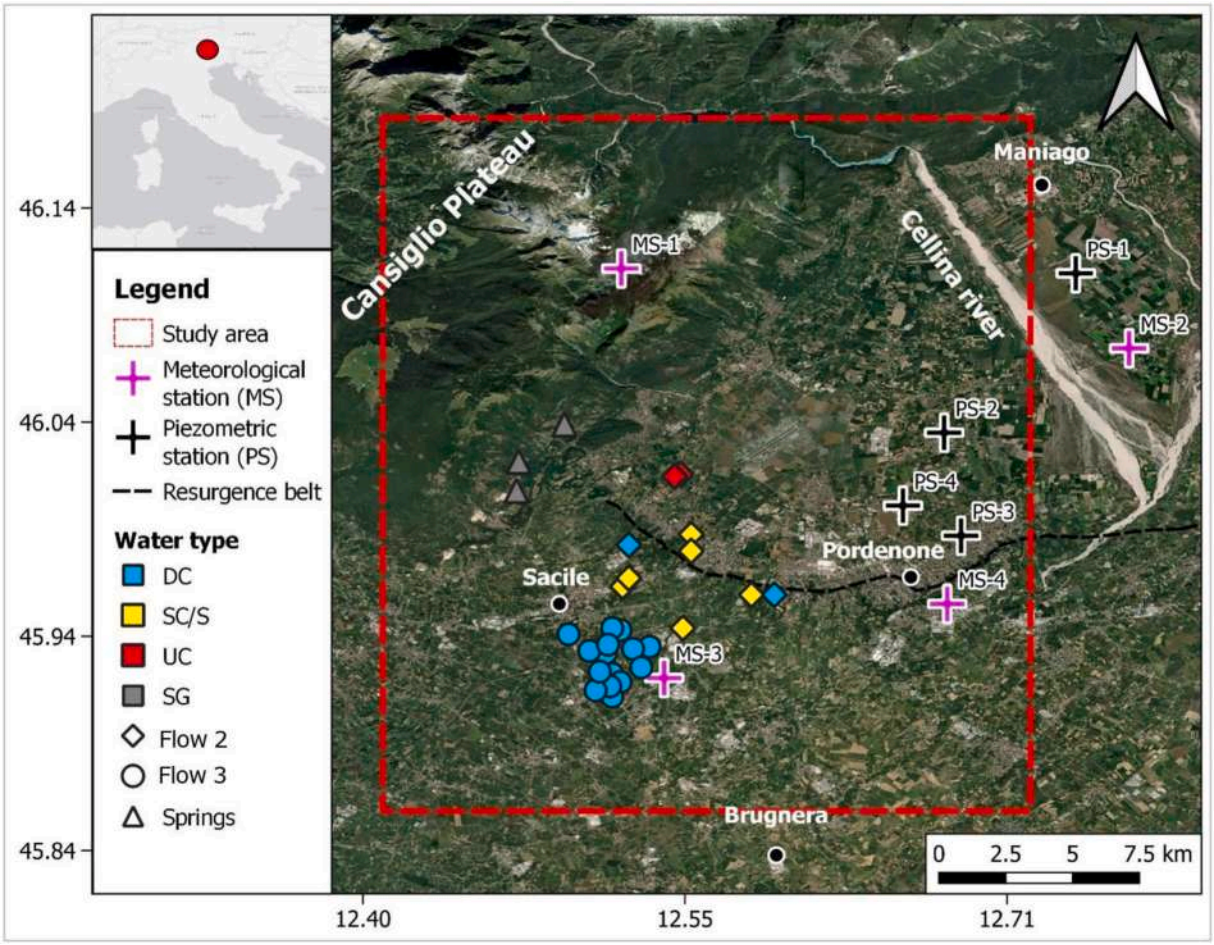


Fig. 2. Location of water samples selected for seasonal monitoring (blu symbol: depth confined aquifers – "DC"; yellow symbol: semi-confined/shallow aquifers – "SC/S"; red symbol: unconfined aquifers – "UC"; grey symbol: spring waters – "SG". Square symbol: data deriving from the Flow 2; circle symbol: data deriving from the Flow 3; triangles symbol: data deriving from the karst springs. MS, meteorological station; PS, piezometric station. Data from ARPA FVG - OSMER and GRN (http://www.meteo.fvg.it/), and Hydraulic Service of the Friuli Venezia Giulia Region. (For interpretation of the references to colour in this figure legend, the reader is referred to the Web version of this article.)

orange as an indicator, with an analytical precision of ±5 mg/L as $CaCO_3$. During sampling, nitrile gloves were worn at all times to minimise contamination, and all sample bottles were rinsed three times with the water being sampled before filling. For isotopic analyses, particular care was taken to minimise contact with the atmosphere. Samples were collected using silicone tubing directly into 50 mL polyethylene bottles, which were filled to the brim and immediately sealed with tight caps to prevent evaporation and isotopic exchange. For major ion analyses, samples were filtered on site using 0.45 μm pore-size membranes and stored in pre-treated 100 mL polyethylene bottles. Samples for anion analysis required no further treatment, whereas samples for cation analysis were acidified with 1% suprapur HNO_3 to prevent precipitation and adsorption phenomena. For $\delta^{18}O$ and $\delta^{2}H$ measurements, unfiltered samples were stored in tightly sealed 50 mL polyethylene bottles. All samples were refrigerated at 4 °C and kept in the dark until laboratory analysis. Geochemical analyses were performed at the Department of Physics and Earth Sciences, University of Ferrara. Anions (Cl^-, NO_3^-, SO_4^{2-}) were measured using a DIONEX ICS-1000 Ion Chromatography System, achieving a relative standard deviation (RSD) of <5%, with detection limits of 0.1 mg/L for Cl^-, 0.05 mg/L for NO_3^-, and 0.1 mg/L for SO_4^{2-}. Cations (Na^+, Mg^{2+}, K^+, Ca^{2+}) were analysed using an iCAP TQ-ICP-MS Triple Quadrupole spectrometer, achieving a RSD of <2% for major elements, with detection limits ranging from 0.01 to 0.1 mg/L depending on the element. Charge balance errors were calculated for all samples and were within ±5%, providing an additional check on the overall analytical consistency of the hydrochemical dataset. Stable isotope measurements for $\delta^{18}O$ and $\delta^{2}H$ were conducted at the Department of Physics and Earth Sciences, University of Ferrara, using a CRDS LWIA 24-d isotopic analyser, with an analytical precision of better than 0.07‰ and 0.2‰, respectively. Results were reported relative to Vienna Standard Mean Ocean Water (V-SMOW).

Quality assurance and quality control (QA/QC) procedures were rigorously applied throughout the analytical process. For ICP-MS analyses, calibration was performed using NIST-traceable multi-element standards, and analytical accuracy was verified through the analysis of certified reference materials. For isotopic measurements, the instrument was calibrated using international reference standards (V-SMOW), and results were normalised to the V-SMOW scale. To monitor analytical drift and ensure data reliability, laboratory blanks (deionised water) were analysed every 10 samples, and no significant contamination was detected. Additionally, 10% of all samples were analysed in duplicate to assess analytical reproducibility, yielding relative differences of less than 3% for major ions and less than 0.1‰ for isotopic ratios.

Thermodynamic calculations were performed using the PHREEQC speciation program (Parkhurst and Appelo, 2013) to assess the chemical speciation of the carbonate system. The calculations involved determining partial pressures of CO_2 (pCO_2) and saturation indices for calcite and dolomite ($SI_{calcite}$ and $SI_{dolomite}$) using pH, alkalinity, temperature, and the main dissolved solutes as input parameters.

Given the limited number of seasonal campaigns (four over two

Table 1
Basic statistics of the groundwater samples belonging to Path 1 within Flow 2. T in °C, EC in μS/cm, TDS total dissolved solids in mg/L, ORP oxidation-reduction potential in mV, Cl^-, NO_3^-, SO_4^{2-}, HCO_3^-, Na^+, Mg^{2+}, K^+, Ca^{2+} in mg/L, pCO_2 in bar (as log), δ^2H, $\delta^{18}O$ and d-excess of H_2O as ‰ V-SMOW. *pH is defined as the negative base-10 logarithm of hydrogen ion activity; therefore, summary statistics were computed by first converting pH values to H^+ activities, calculating the statistics on the activity scale, and then transforming the results back to pH.

	*pH	T	EC	Cl^-	NO_3^-	SO_4^{2-}	HCO_3^-	Na^+	Mg^{2+}	K^+	Ca^{2+}	pCO_2	δ^2H	$\delta^{18}O$	d-excess	$SI_{Calcite}$	$SI_{Dolomite}$
Summer 2021																	
Min.	7.45	9.1	180	2.5	3.9	1.9	146	0.8	1.5	0.41	43.1	−2.56	−59.39	−10.13	15.16	−0.26	−1.57
Max.	7.77	11.3	216	2.9	4.0	2.7	160	1.4	2.0	0.46	48.9	−2.27	−51.24	−8.87	24.24	0.13	−0.91
Median	7.70	10.9	188	2.8	4.0	2.3	150	1.0	1.7	0.45	43.8	−2.54	−55.78	−9.43	21.40	−0.06	−1.30
SD (±)	0.17	1.2	19	0.2	0.02	0.4	7	0.3	0.3	0.03	3.2	0.16	4.08	0.63	4.64	0.20	0.33
Winter 2021																	
Min.	7.13	9.13	141	2.1	3.7	2.7	120	0.8	1.2	0.41	37.5	−2.17	−58.6	−8.70	8.28	−0.68	−2.54
Max.	7.25	10.9	197	2.7	4.5	2.9	130	1.0	1.4	0.44	40.1	−2.01	−51.8	−8.01	14.36	−0.63	−2.44
Median	7.20	10.3	183	2.5	4.2	2.9	125	0.9	1.3	0.41	38.5	−2.10	−55.8	−8.27	11.00	−0.66	−2.47
SD (±)	0.06	0.9	29	0.3	0.4	0.1	5	0.1	0.1	0.02	1.3	0.08	3.41	0.35	3.05	0.03	0.05
Summer 2022																	
Min.	7.59	9.9	205	1.7	2.1	1.9	170	0.8	1.6	0.45	49.1	−2.70	−59.9	−8.91	10.22	0.07	−0.95
Max.	7.96	12.1	241	2.1	3.6	2.6	190	1.4	2.2	0.47	53.4	−2.30	−52.1	−8.29	16.30	0.39	−0.38
Median	7.86	11.8	232	2.1	3.0	2.5	180	1.1	1.8	0.46	52.3	−2.63	−56.1	−8.55	11.38	0.22	−0.76
SD (±)	0.19	1.2	19	0.2	0.7	0.4	10	0.3	0.3	0.01	2.3	0.21	3.91	0.31	3.23	0.16	0.29
Winter 2022																	
Min.	7.30	9.4	152	2.0	3.4	2.3	120	0.8	1.4	0.42	36.9	−2.30	−58.8	−8.64	10.22	−0.55	−2.17
Max.	7.40	10.7	201	2.4	3.5	3.4	130	0.9	1.6	0.44	39.4	−2.18	−52.1	−8.09	14.30	−0.47	−2.09
Median	7.34	9.4	176	2.2	3.4	2.5	125	0.8	1.4	0.42	38.0	−2.26	−54.5	−8.30	10.32	−0.52	−2.12
SD (±)	0.05	0.7	25	0.2	0.05	0.6	5	0.1	0.2	0.01	1.3	0.06	3.38	0.28	2.33	0.04	0.04

Table 2
Basic statistics of the groundwater samples belonging to Path 2 – Group 1 within Flow 2. T in °C, EC in mS/cm, TDS total dissolved solids in mg/L, ORP oxidation-reduction potential in mV, Cl^-, NO_3^-, SO_4^{2-}, HCO_3^-, Na^+, Mg^{2+}, K^+, Ca^{2+} in mg/L, pCO_2 in bar (as log), δ^2H, $\delta^{18}O$ and d-excess of H_2O as ‰ V-SMOW. *pH is defined as the negative base-10 logarithm of hydrogen ion activity; therefore, summary statistics were computed by first converting pH values to H^+ activities, calculating the statistics on the activity scale, and then transforming the results back to pH.

	*pH	T	EC	Cl^-	NO_3^-	SO_4^{2-}	HCO_3^-	Na^+	Mg^{2+}	K^+	Ca^{2+}	pCO_2	δ^2H	$\delta^{18}O$	d-excess	$SI_{Calcite}$	$SI_{Dolomite}$
Summer 2021																	
Min.	7.26	12.7	320	3.0	5.7	3.4	185	1.1	17.0	0.3	42.3	−2.70	−56.6	−8.82	1.60	−0.10	−0.24
Max.	8.02	14.7	597	5.2	36.0	9.8	250	2.9	27.7	1.0	61.4	−1.85	−50.8	−6.55	14.76	0.42	0.81
Median	7.80	13.1	357	3.2	6.9	4.0	205	1.3	19.1	0.5	46.3	−2.49	−55.3	−8.24	10.82	0.22	0.31
SD (±)	0.26	0.8	105	0.8	12.0	2.5	27	0.7	4.1	0.2	7.0	0.29	2.04	0.82	4.79	0.20	0.40
Winter 2021																	
Min.	7.15	11.2	225	2.7	5.7	3.2	180	0.9	15.6	0.3	38.2	−2.35	−56.1	−8.53	0.20	−0.33	−0.73
Max.	7.63	12.1	417	4.5	24.9	10.0	240	2.1	22.2	1.0	52.9	−1.77	−50.6	−6.35	12.24	0.07	0.08
Median	7.58	11.4	280	2.9	6.7	4.0	195	1.0	17.4	0.4	43.9	−2.28	−54.8	−8.02	9.77	−0.06	−0.22
SD (±)	0.19	0.3	71	0.7	7.5	2.6	26	0.5	2.8	0.3	5.2	0.22	2.02	0.81	4.76	0.15	0.31
Summer 2022																	
Min.	7.55	12.1	309	3.4	6.1	3.6	200	1.1	18.9	0.4	40.8	−2.58	−57.0	−8.88	2.40	0.02	−0.07
Max.	7.90	13.9	522	6.0	40.8	11.1	270	2.8	30.7	1.0	67.2	−2.22	−51.2	−6.70	14.38	0.32	0.61
Median	7.68	12.8	352	3.9	8.0	4.5	210	1.5	20.3	0.5	48.6	−2.32	−55.4	−8.36	11.69	0.24	0.42
SD (±)	0.13	0.6	78	0.9	13.7	2.9	27	0.7	4.6	0.2	8.9	0.14	2.04	0.84	4.84	0.13	0.30
Winter 2022																	
Min.	7.10	10.1	225	2.1	5.4	2.6	180	0.7	14.0	0.2	36.7	−2.28	−55.9	−8.41	−0.30	−0.46	−1.07
Max.	7.56	11.9	320	3.1	20.4	7.7	260	2.0	26.7	1.6	58.8	−1.69	−49.9	−6.20	11.44	−0.15	−0.35
Median	7.35	11.1	257	2.4	5.5	3.1	187	1.2	16.3	0.4	40.8	−2.03	−54.0	−7.92	9.51	−0.27	−0.62
SD (±)	0.16	0.7	37	0.4	6.0	1.9	33	0.4	4.7	0.5	8.3	0.21	1.99	0.82	4.74	0.12	0.27

years), formal statistical hypothesis testing (e.g., repeated-measures ANOVA or the Friedman test) was not applied, as such a small sample size would provide insufficient statistical power to draw robust inferences. Seasonal variations were therefore evaluated descriptively, considering their magnitude, direction, and consistency with the hydrogeological conceptual model.

4. Results and discussion

4.1. Seasonal hydro-meteorological characterization

To investigate the hydrogeochemical variations of the PP hydrogeological system in response to seasonal changes, it is important to analyse the hydro-meteorological variations recorded in the study area. Detailed seasonal temperature and precipitation data are provided in Table 3S. By examining the available climate data, temperature and precipitation patterns in 2021 and 2022 were characterized across the

Table 3
Basic statistics of the groundwater samples belonging to Path 2 – Group 2 within Flow 2. T in °C, EC in mS/cm, TDS total dissolved solids in mg/L, ORP oxidation-reduction potential in mV, Cl^-, NO_3^-, SO_4^{2-}, HCO_3^-, Na^+, Mg^{2+}, K^+, Ca^{2+} in mg/L, pCO_2 in bar (as log), δ^2H, $\delta^{18}O$ and d-excess of H_2O as ‰ V-SMOW. *pH is defined as the negative base-10 logarithm of hydrogen ion activity; therefore, summary statistics were computed by first converting pH values to H^+ activities, calculating the statistics on the activity scale, and then transforming the results back to pH.

	*pH	T	EC	Cl^-	NO_3^-	SO_4^{2-}	HCO_3^-	Na^+	Mg^{2+}	K^+	Ca^{2+}	pCO_2	δ^2H	$\delta^{18}O$	d-excess	$SI_{Calcite}$	$SI_{Dolomite}$
Summer 2021																	
Min.	7.21	11.2	200	1.4	0.9	1.2	180	1.5	18.3	0.3	27.1	−2.39	−63.3	−9.09	6.54	−0.63	−1.12
Max.	7.72	13.6	502	2.5	5.2	5.8	270	3.1	25.3	0.7	60.9	−1.88	−54.0	−7.73	10.92	0.16	0.27
Median	7.50	12.8	283	2.3	4.0	4.2	237	2.0	20.8	0.4	45.4	−2.08	−58.5	−8.56	9.34	0.08	0.08
SD (±)	0.20	1.0	109	0.5	2.1	2.2	31	0.6	3.0	0.1	12.2	0.19	3.89	0.56	1.60	0.31	0.54
Winter 2021																	
Min.	7.52	12.1	263	2.0	2.8	3.3	190	1.6	20.1	0.5	29.2	−2.51	−65.2	−10.1	7.82	−0.08	−0.12
Max.	7.80	15.1	404	3.2	14.0	20.5	285	4.2	29.4	0.6	62.3	−2.05	−58.6	−8.84	19.08	0.39	0.60
Median	7.65	13.5	356	2.5	7.1	9.4	252	2.2	20.5	0.5	48.1	−2.27	−64.2	−9.83	15.47	0.19	0.34
SD (±)	0.11	1.2	52	0.5	4.8	7.2	37	0.9	4.0	0.1	12.9	0.16	2.42	0.47	3.76	0.17	0.26
Summer 2022																	
Min.	7.14	11.6	203	1.3	2.6	2.8	170	1.3	17.8	0.4	28.1	−2.26	−63.5	−9.32	9.46	−0.70	−1.30
Max.	7.63	14.1	487	2.5	6.5	6.4	260	3.6	26.3	0.7	59.6	−1.77	−54.8	−8.17	12.86	0.06	0.18
Median	7.20	12.8	274	1.9	6.2	4.7	237	2.1	20.2	0.4	45.8	−1.83	−59.5	−8.88	10.70	−0.25	−0.58
SD (±)	0.19	0.9	99	0.5	2.7	2.4	32	0.8	3.6	0.1	11.5	0.19	3.54	0.42	1.12	0.26	0.47
Winter 2022																	
Min.	7.41	12.2	245	1.6	2.3	2.9	195	1.6	19.2	0.4	30.2	−2.51	−65.2	−10.3	8.36	−0.17	−0.31
Max.	7.82	14.7	431	2.8	6.9	12.1	290	4.2	30.1	0.6	61.9	−2.00	−58.9	−8.92	19.10	0.30	0.45
Median	7.55	13.9	344	2.1	6.0	6.4	257	2.2	21.3	0.5	48.1	−2.17	−64.4	−9.99	16.60	0.08	0.27
SD (±)	0.14	1.1	66	0.5	2.7	4.2	38	0.9	4.4	0.1	12.6	0.18	2.36	0.52	3.79	0.16	0.31

two distinct sectors of the PP. In agreement with ARPA FVG-OSMER (2018), the 2nd and 3rd trimesters were the warmest periods of the year. A clear distinction was observed between the CPA sector and the plain sectors (HP and LP). Average annual temperatures recorded at the Piancavallo station (MS-1), in the CPA, are generally 8–10 °C lower than those in the plain. Considering the interannual variation between the 2021 and 2022, the year 2022 was generally warmer than 2021, as evidenced by the significant drought that affected the Friuli-Venezia Giulia region in 2022 (ARPA FVG-OSMER, 2023). Specifically, the CPA showed an average temperature increase of approximately 2 °C, excluding the 3rd trimester, while the plain sector experienced an increase of 1–3 °C, except during the 1st trimester. Rainfall data reveal higher precipitation during the 2nd and 4th trimesters, with a marked decrease in 2022 compared to 2021. In agreement with ARPA-OSMER, 2008, compared with 2021, the plain recorded an average annual decrease in precipitation of 2–3 mm during the 1st and 2nd trimesters, while the CPA sector showed a decrease of 3–4 mm. The 3rd trimester exhibited negligible variation, whereas the 4th trimester showed a reduction of 1–1.5 mm annually across both sectors. Temporal trends in precipitation at the reference stations for the period 2021–2022 are presented in Fig. 1S. Regarding snowfall data, the analysis focused on records from the MS-1 station, located in the CPA sector. In accordance with ARPA FVG-OSMER (2018), as shown in Fig. 3a, the 1st and 4th trimesters are characterized by the highest snow-cover values. Moreover, despite the incomplete dataset, a marked reduction in snow cover in 2022 is evident. Snow cover decreased from an average of 100 cm in the 1st trimester of 2021 to approximately 40 cm in the 4th trimester of 2021 and 30 cm in the 1st trimester of 2022. This decreasing trend in both rainfall and snowfall may have affected the hydrogeological system of the PP, as the system relies on mountain recharge areas where snowmelt and rainfall play a fundamental role in sustaining groundwater resources (Cucchi et al., 2008; Zini et al., 2011; Di Renzo et al., 2023).

In the PP, the piezometric level of the phreatic aquifer in the HP has demonstrated a significant and sustained decline over the past three decades, with an estimated reduction of approximately 0.1–0.4 m/year (Cucchi et al., 1999; Calligaris et al., 2010; Zini et al., 2013). This decline is predominantly attributed to diminished recharge inputs due to reduced rainfall and snowfall, increased groundwater extraction for domestic, agricultural, and industrial purposes, and the extensive exploitation of mountain water resources for irrigation and hydropower (DiSGAM, 2006; ARPA FVG, 2012).

An analysis of piezometric variations in the HP aquifer, based on data recorded between January 2020 and March 2023 (Fig. 2S), indicates a marked decline in piezometric levels beginning in the summer of 2021 and persisting until the end of 2022. This reduction appears to have been intensified by drought conditions during 2022. A comparison of the piezometric trend in the HP aquifer with precipitation patterns recorded at the Piancavallo meteorological station in the CPA reveals a clear qualitative co-variation between these variables, reflecting a consistent hydrological response to recharge events. As illustrated in Fig. 3b, piezometric levels in the HP aquifer demonstrate a rapid response to changes in precipitation patterns, albeit with a lag of approximately two months. Within this overall declining trend, Fig. 3b highlights distinct periods of higher and lower piezometric levels between 2021 and 2022, characterized by well-defined peaks and troughs.

i) The first period of maximum piezometric levels spans from January 2021 to March 2021, followed by a short period of minimum piezometric level in May-June 2021.
ii) A second period of maximum piezometric levels is recorded in July 2021, followed by a decrease in the piezometric level, reaching its minimum in November 2021.
iii) A third period of maximum piezometric levels occurs in January 2022, followed by a decrease in the piezometric level until November-December 2022.

4.2. *Seasonal geochemical/isotopic characterization of the flow 2*

4.2.1. *Flow 2: path 1 – karst springs*

The results obtained by Di Renzo et al. (2024) highlight a consistent co-variation between the chemistry of karst spring waters and the rainfall and snowfall patterns characteristic of the Cansiglio Plateau area, which represents a key recharge zone for the aquifer systems of the area. To compare the seasonal geochemical and isotopic variations with recorded snowfall and rainfall patterns for 2021 and 2022 in this

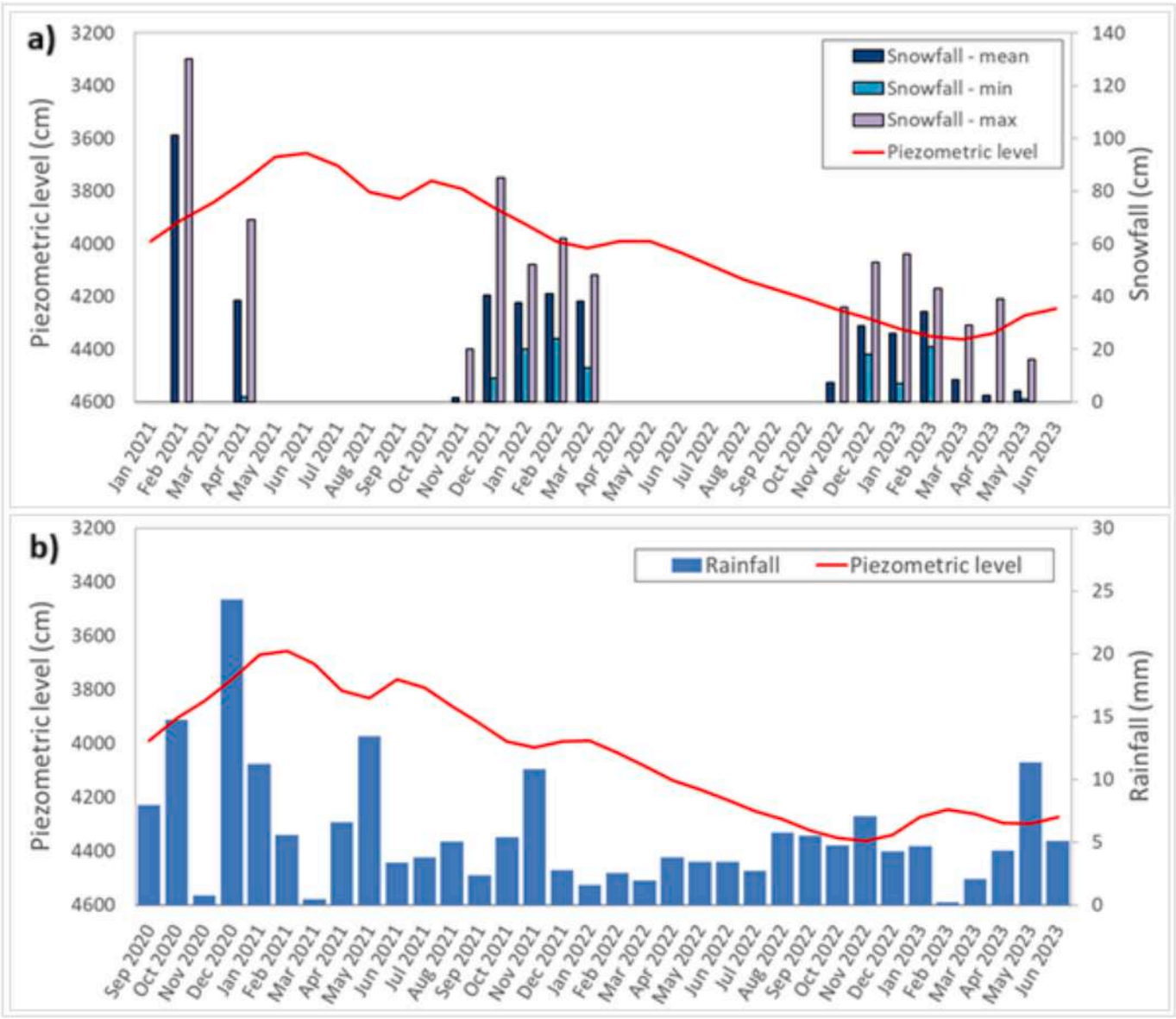


Fig. 3. Comparison between snowfall (a) and rainfall (b) in the MS-1 station and piezometric level of HP phreatic aquifer relative to the local topographic surface.

recharge area, the MS-1 station was selected as a reference point (Fig. 2).

The study of seasonal geochemical and isotopic variations focused on two distinct periods: the intra-recharge period (June–July 2021/2022), marked by reduced recharge inputs, high evapotranspiration, and occasional influence from the final phase of snowmelt (hereafter referred to as the summer or dry period), and the recharge period (November–December 2021/2022), dominated by substantial recharge from autumnal rainfall (hereafter referred to as the winter or wet period). The seasonal variations observed along Path 1 of Flow 2 in the main physicochemical parameters, major ions, stable water isotopic compositions, pCO_2, as well as calcite and dolomite saturation indices are reported in Table 4S. Descriptive statistics for the seasonal geochemical survey are presented in Table 1.

The analyses reveal seasonal variations of different magnitudes among the parameters examined between the summer and winter periods. Moreover, the drought affecting the study area from late 2021 through autumn 2022 resulted in pronounced differences between the summer periods of 2021 and 2022. Among the chemical/physical parameters, pH, temperature (T), and electrical conductivity (EC) showed the most marked seasonal variation. The pH values fall within the neutral-alkaline range, with median values of 7.70 for summer 2021, 7.20 for winter 2021, 7.78 for summer 2022, and 7.34 for winter 2022. In both winter periods, a decrease in pH was observed following autumnal rainfall and the associated recharge. This could be attributed to the mixing of pre-existing waters with the recharge input from autumnal precipitation. It is known that precipitation generally has a more acidic pH (at a value around 5.60) due to dissolved atmospheric CO_2. With recharge events, atmospheric CO_2 reacts with water, producing carbonic acid (H_2CO_3), thus leading to a decrease in pH. This phenomenon is well documented in the literature as the contribution of acidic rainwaters during major rain-discharge events in karst springs (Zhao et al., 2010; Colombo et al., 2015; Setiawan et al., 2019; Khudair et al., 2022). Additionally, Liu et al. (2004) and He et al. (2023) highlight that rainwater can dissolve carbon dioxide in the soil, further increasing the contribution of CO_2 during infiltration. This interpretation is consistent with the calculated pCO_2 values, which are higher during rainy periods and lower during the summer period, specifically in 2022. In detail, the pCO_2 values show a median of −2.54 (log bar) in summer 2021, -2.10 (log bar) in winter 2021, -2.63 (log bar) in summer 2022, and -2.26 (log bar) in winter 2022. Dissolved CO_2, despite the lack

Table 4
Basic statistics of the groundwater samples belonging to Flow 3. T in °C, EC in mS/cm, TDS total dissolved solids in mg/L, ORP oxidation-reduction potential in mV, Cl^-, NO_3^-, SO_4^{2-}, HCO_3^-, Na^+, Mg^{2+}, K^+, Ca^{2+} in mg/L, pCO_2 in bar (as log), δ^2H, $\delta^{18}O$ and d-excess of H_2O as ‰ V-SMOW. *pH is defined as the negative base-10 logarithm of hydrogen ion activity; therefore, summary statistics were computed by first converting pH values to H^+ activities, calculating the statistics on the activity scale, and then transforming the results back to pH. "b.d.l.": below detection limit.

	*pH	T	EC	Cl^-	NO_3^-	SO_4^{2-}	HCO_3^-	Na^+	Mg^{2+}	K^+	Ca^{2+}	pCO_2	δ^2H	$\delta^{18}O$	d-excess	$SI_{Calcite}$	$SI_{Dolomite}$
Summer 2021																	
Min.	7.15	15.9	306	1.6	b.d.l.	b.d.l.	280	39.9	7.0	3.8	35.4	−2.23	−76.5	−11.7	8.38	−0.21	−0.63
Max.	7.78	20.4	715	2.4	b.d.l.	b.d.l.	360	66.8	20.3	8.8	49.6	−1.61	−68.3	−9.91	20.10	0.47	0.71
Median	7.35	17.9	377	2.1	b.d.l.	b.d.l.	330	50.7	13.0	5.1	41.4	−1.87	−71.1	−10.6	14.70	0.09	−0.02
SD (±)	0.21	1.5	95	0.2	b.d.l.	b.d.l.	26	8.8	3.7	1.3	4.5	0.21	2.41	0.60	3.62	0.24	0.45
Winter 2021																	
Min.	7.01	14.3	289	1.7	b.d.l.	b.d.l.	280	38.7	7.4	3.9	33.4	−2.15	−76.1	−12.0	8.13	−0.31	−0.84
Max.	7.69	19.5	687	2.6	b.d.l.	b.d.l.	370	61.2	19.4	8.5	52.5	−1.44	75.4	−10.0	23.50	0.39	0.47
Median	7.32	17.2	351	2.2	b.d.l.	b.d.l.	325	48.3	12.0	4.8	40.3	−1.77	−71.4	−10.7	14.85	0.01	−0.23
SD (±)	0.21	1.6	95	0.2	b.d.l.	b.d.l.	27	6.7	3.4	1.1	5.4	0.22	36.8	0.57	4.27	0.21	0.41
Summer 2022																	
Min.	7.11	15.8	297	1.3	b.d.l.	b.d.l.	270	40.1	7.0	3.9	35.2	−2.18	−75.8	−11.9	8.93	−0.24	−0.68
Max.	7.75	20.2	741	2.5	b.d.l.	b.d.l.	365	59.8	19.1	7.9	48.4	−1.56	75.6	−9.94	22.10	0.48	0.74
Median	7.38	17.7	362	2.2	b.d.l.	b.d.l.	330	47.6	12.4	5.0	40.0	−1.88	−70.7	−10.7	14.04	0.00	−0.14
SD (±)	0.20	1.4	102	0.3	b.d.l.	b.d.l.	27	6.6	3.3	1.0	4.3	0.20	49.5	0.59	3.95	0.21	0.43
Winter 2022																	
Min.	7.10	15.2	318	1.6	b.d.l.	b.d.l.	285	38.8	7.2	4.0	34.1	−2.25	−76.7	−11.9	8.08	−0.26	−0.67
Max.	7.80	20.1	721	2.5	b.d.l.	b.d.l.	360	62.5	20.4	8.0	49.2	−1.51	75.8	−10.0	22.60	0.49	0.66
Median	7.35	17.6	382	2.0	b.d.l.	b.d.l.	333	48.8	12.2	4.9	40.6	−1.85	−71.5	−10.8	14.45	0.01	−0.26
SD (±)	0.22	1.5	94	0.2	b.d.l.	b.d.l.	27	7.4	3.4	1.0	4.5	0.22	49.9	0.58	4.06	0.24	0.46

of corresponding carbon-isotope data, may therefore have a predominantly soil-derived component, with values closer to the reported soil-derived CO_2 values (log (bar) = −2.00, e.g. Drever, 1997) than to the atmospheric value (log bar = −3.50, Hem, 1989). This soil-derived CO_2 interpretation is further corroborated by carbon isotope data from Donnini et al. (2026), who reported a mean $\delta^{13}C$ value of −10.29‰ for dissolved inorganic carbon in the studied karst waters. This intermediate isotopic signature is consistent with the expected mixing between soil-respired CO_2 ($\delta^{13}C \approx -25$‰, typical of C3 vegetation in the region) and marine carbonate minerals ($\delta^{13}C \approx 0$‰) during water-rock interaction. The influence of recharge input due to autumnal rainfall is also observed, in accordance with Filippini et al. (2018), in the variations in T and EC. During the winter period, a decrease in both parameters is registered, indicating the contribution of relatively cold, low-mineralisation recharge water. In particular, the T and EC show median values of 10.9 °C and 188 μS/cm for summer 2021; 10.3 °C and 183 μS/cm for winter 2021; 11.8 °C and 232 μS/cm for summer 2022; and 9.4 °C and 176 μS/cm for winter 2022. This reduction in T and EC in karst springs is common during recharge periods (Wang et al., 2020; De Filippi et al., 2021; Balestra et al., 2022; Nannoni and Piccini, 2022; Torresan et al., 2022). An exception to this seasonal trend was recorded at SG-3 (Table 4S). In line with Filippini et al. (2018), the piston flow phenomenon characterising this spring may account for the increase in EC following recharge periods. This increase is particularly evident during the winter period influenced by autumnal precipitation recharge. However, the exceptional drought conditions during 2021-2022 also markedly affected these parameters, particularly during the summer of 2022. The scarcity of snowfall, mainly in late 2021 and early 2022, coupled with reduced rainfall, likely resulted in reduced recharge and consequently contributed to the higher T and EC values observed during summer 2022. Fig. 3S illustrates the effect of drought on spring SG-1. The seasonal trends of the major ions for the three springs show that HCO_3^- and Ca^{2+} are the most abundant species and exhibit pronounced seasonal variations among the different surveys. The HCO_3^- and Ca^{2+} values show a median, respectively, of 150 and 43.8 mg/l in summer 2021; 125 and 38.5 mg/l in winter 2021; 180 and 52.3 mg/l in summer 2022; and 125 and 38.0 mg/l in winter 2022. Mg^{2+} values also show notable seasonal variation, albeit with lower concentrations. In particular, the Mg^{2+} values show a median concentration of 1.7 mg/l in summer 2021, 1.3 mg/l in winter 2021, 1.8 mg/l in summer 2022, and 1.3 mg/l in winter 2022. The SO_4^{2-} and NO_3^- concentrations are relatively low and exhibit a slight seasonal variation. The SO_4^{2-} and NO_3^- values show a median, respectively, of 2.3 and 4.0 mg/l in summer 2021; 3.0 and 4.2 mg/l in winter 2021; 2.5 and 3.0 mg/l in summer 2022; and 2.5 and 3.4 mg/l in winter 2022. In contrast, Cl^-, Na^+ and K^+ do not exhibit pronounced seasonal variations.

Fig. 4a graphically illustrates the seasonal variation in ionic concentrations. The ions exhibiting substantial variability are HCO_3^-, Mg^{2+}, and Ca^{2+}, in accordance with the Ca-HCO_3 nature of these spring waters, as described by Di Renzo et al. (2024). Although the fundamental Ca-HCO_3 hydrochemical facies is maintained throughout the seasonal cycle, the relative proportions of major ions exhibit distinct shifts in response to changes in recharge dynamics. Winter recharge events induce a dilution effect that temporarily shifts the chemical signature toward less mineralised meteoric recharge, while summer periods, particularly under drought conditions. These circumstances may enhance water-rock interaction and reduce the water–rock ratio, leading to higher concentrations of dissolved solutes (Fig. 4Sa). Consistent with these variations, EC values increase during the summer period and decrease during the winter period. The decrease in EC during the winter period can be attributed to the effect of recharge from autumnal rainfall, which leads to a dilution effect within the aquifer system (Liu et al., 2007, 2019; Zhao et al., 2010; Dar et al., 2015; Guo et al., 2022). Notably, during the summer period of 2022, the concentrations of HCO_3^-, Na^+, Mg^{2+}, K^+, and Ca^{2+} increased compared to the summer period of 2021. These results are consistent with the drought conditions of 2022, characterised by reduced snowfall and rainfall, especially in the first half of the year. The variations in Mg^{2+} concentration during the summer period are more pronounced in SG-1 compared to SG-2 and SG-3, consistent with Filippini et al. (2018). This pattern is consistent with the nature of the SG-1 groundwater source, which is partially fed by dolomitic rocks present in the deeper part of the system and in proximity to Mt. Piancavallo.

The saturation index (SI) of calcite and dolomite shows a seasonal variation and clearly reflects the effect of recharge from autumnal rainfall. In detail, the SI of calcite and dolomite values show a median,

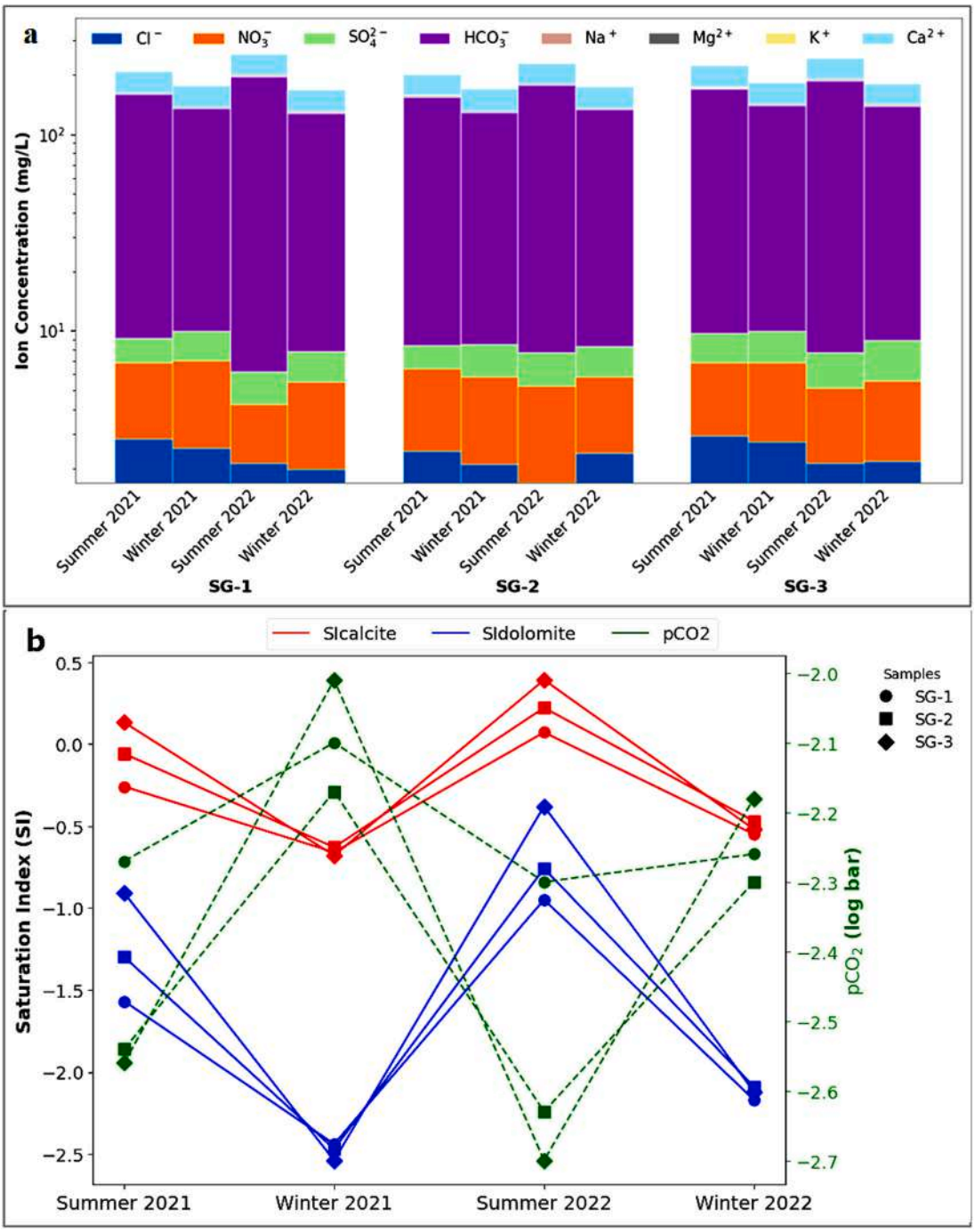


Fig. 4. The seasonal trends of the major ions (a), pCO_2 and saturation Index (SI) of calcite and dolomite (b), and $\delta^{18}O$ (c) for the Flow 2- Path 1.

respectively, of −0.06 and −1.30 in summer 2021; −0.66 and −2.47 in winter 2021; 0.22 and −0.76 in summer 2022; −0.52 and −2.12 in winter 2022. Fig. 4b indicates that during the winter period, both SIs tend towards undersaturation. This pattern is consistent with the dilution effect caused by new recharge (Liu et al., 2007; Naoura et al., 2021; Çelik et al., 2022). Conversely, during the summer periods, the SIs shows more positive values, particularly for calcite, tending towards saturation, in accordance with the Ca-HCO_3 nature of the springs. The impact of the 2022 summer drought is notable, leading to an increase in both calcite and dolomite saturation indices compared to the summer period of 2021. Finally, Fig. 4b reveals that during the summer periods, the SIs are higher in SG-1 and lower in SG-3. This differentiation could be attributed to the varying distances between the recharge area and the surface outlet of the springs, as identified by Vincenzi et al. (2011) and Filippini et al. (2018). Specifically, SG-3 has a single recharge area proximal to the spring, SG-2 has multiple recharge areas both proximal and distal to the spring, and SG-1 has a single recharge area in the distal part of the system. This interpretation is also supported by the Ca/Mg ratio of the springs, which tends to decrease with increasing distance between the recharge area(s) and the spring outlet. Indeed, due to the different dissolution kinetics of calcite (faster) and dolomite (slower), when waters do not receive a new recharge input, as in summer periods, they have time to interact with sediments and dissolve carbonate minerals, including dolomite, and subsequently, the Ca/Mg ratio tends to be

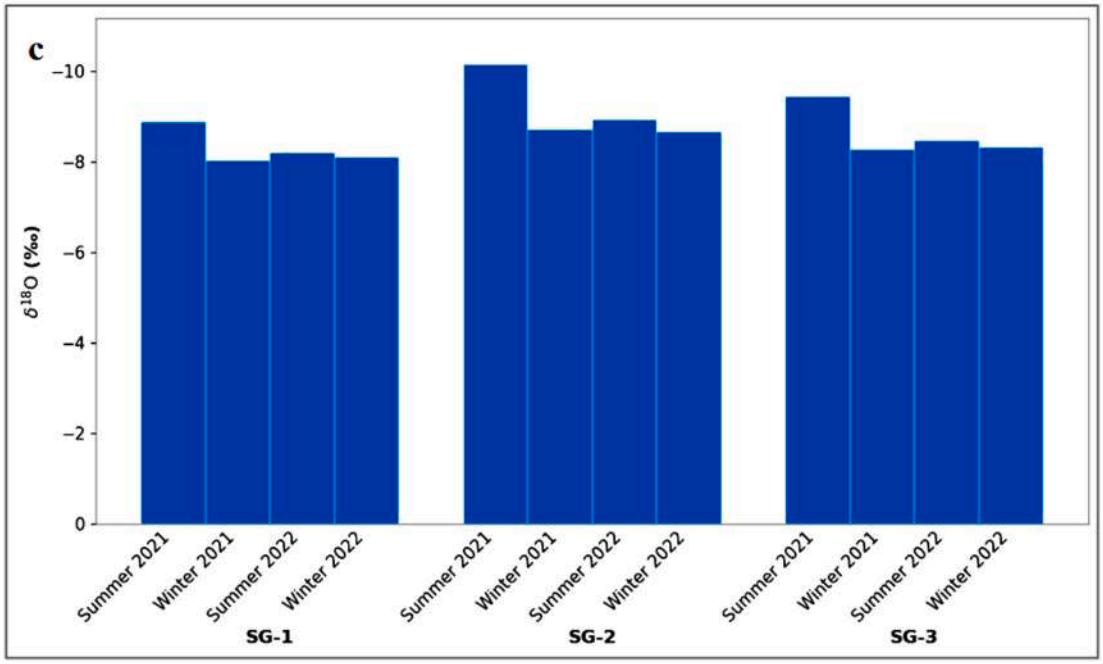


Fig. 4. (*continued*).

low. In karst springs, seasonal variations in the stable hydrogen and oxygen isotope composition of water are commonly observed and can be used to characterise rapid responses from recharge to discharge processes (Mance et al., 2014; Hu et al., 2015; Jeelani et al., 2015; Malík et al., 2015; Cao et al., 2018; Palcsu et al., 2021; Ansari et al., 2022).

The isotopic values of $\delta^{18}O$ and $\delta^{2}H$ during the seasonal study show median values, respectively, of −9.43 and −55.8‰ in summer 2021; −8.27 and −55.8‰ in winter 2021; −8.55 and −56.1‰ in summer 2022; −8.30 and −54.5‰ in winter 2022. Fig. 4c illustrates the seasonal variation in $\delta^{18}O$, which follows the snowfall and rainfall regimes recorded in the Cansiglio Plateau area, consistent with Filippini et al. (2018). A marked $\delta^{18}O$ depletion was observed in all three springs during summer 2021, which may be attributed to the contribution of snowmelt recharge. However, this effect is not evident during the summer of 2022, when snowfall was substantially reduced. With a diminished snow-driven recharge rate, a pronounced depletion in $\delta^{18}O$ values was not recorded, suggesting a shift in the isotopic composition of recharge under drought conditions (Noble and Ansari, 2019; Ansari et al., 2020). Conversely, during the winter periods, isotopic enrichment is observed, which is consistent with rainfall-dominated recharge, as reported by Barbieri et al. (2005), Abbott et al. (2000), Filippini et al. (2018), and Lucianetti et al. (2020).

To further constrain the recharge processes and evaluate potential evaporation, mixing and renewability, stable isotope data were integrated with conservative tracers such as chloride and the deuterium excess (d-excess = $\delta^{2}H - 8 \times \delta^{18}O$, Dansgaard, 1964). The seasonal dataset reveals a distinct hydrological signature: summer 2021 samples exhibit the most depleted $\delta^{18}O$ and $\delta^{2}H$ values coupled with exceptionally high d-excess values (ranging from 15.1‰ to 24.2‰ across the springs; Fig. 4Sb). This elevated d-excess is consistent with a contribution from snowmelt recharge, potentially reflecting kinetic fractionation processes during snow formation in the high-altitude catchment (Sprenger et al., 2024). The stark contrast between summer 2021 and the drought-affected summer 2022 provides further evidence of changes in the seasonal recharge regime. In summer 2022, the d-excess values decreased toward the range generally observed for meteoric waters (10–16‰), while $\delta^{18}O$ became slightly enriched, consistent with the reduced contribution of snowmelt to recharge. The relationship between d-excess and Cl^{-} (Fig. 4Sc) provides additional evidence that significant post-recharge evaporation is unlikely to be the main driver of the observed isotopic variability. If evaporation were the dominant driver of the 2022 summer chemistry, a decrease in d-excess would generally be expected to occur together with enrichment of conservative solutes such as Cl^{-}. Instead, the data show that the lower summer 2022 d-excess values coincide with stable or decreasing Cl^{-} levels. This pattern supports the interpretation that the observed isotopic shifts primarily reflect changes in the meteoric recharge source, particularly the reduced contribution of snowmelt, rather than substantial in-aquifer evaporation. Furthermore, the rapid convergence of d-excess values toward the range characteristic of local meteoric recharge during both winter 2021 and winter 2022, accompanied by stable Cl^{-} concentrations, is consistent with the rapid contribution of rainfall-dominated recharge. This seasonal resetting of the isotopic and chemical baseline, even following the severe summer drought, indicates a rapid hydraulic response of these karst springs to changes in surface recharge conditions and supports their high degree of hydrological renewability.

Overall, these findings advance the understanding of karst-alluvial interactions by demonstrating how the hydrochemical signature of these springs is highly sensitive to the shifting balance between snowmelt and rainfall recharge, a defining feature of the Cansiglio Plateau recharge system. The absence of the typical summer snowmelt isotopic depletion in 2022 highlights a potential vulnerability of the system: as climate change reduces snowpack accumulation, these systems may progressively lose part of the seasonal snowmelt contribution that currently provides a natural dilution input. This could favour higher solute concentrations and modify water–rock interaction dynamics, including the relative contribution of dolomite dissolution, under prolonged low-recharge conditions, consistent with observations from other alpine and mountainous karst systems (Kanduč et al., 2012; Masiol et al., 2026; Rispal et al., 2026). These findings highlight the importance of seasonal monitoring for detecting hydroclimatic changes and their effects on groundwater chemistry, thereby providing a robust baseline for sustainable water-resource management (Kumar and Ansari, 2021).

4.2.2. *Flow 2: path 2 - groundwater pathway within the plain*

The results obtained by Di Renzo et al. (2024) highlighted a secondary pathway within Flow 2 that contributes to the recharge of aquifers located in the plain, particularly the unconfined aquifers (UC)

in the HP and the shallow semi-confined aquifers (SC/S) located near the resurgence belt. To examine the seasonal geochemical and isotopic variations along this flow, sampling points representing different aquifers at various depths and spatial locations were selected.

Detailed seasonal trends at the monitoring points associated with Path 2 of Flow 2 are presented in Table 5S. The data reveal that seasonal variations in physicochemical, hydrogeochemical, and isotopic parameters are not confined to specific aquifer types but are instead influenced by their spatial distribution and position within the hydrogeological system. Based on their spatial and hydrogeological relationships, this path can be divided into two groups, with the resurgence belt representing a key hydrogeological boundary (Fig. 5). Group 1 comprises three wells in the UC of the HP (UC-1, UC-2, UC-3) and three wells in the semi-confined/shallow aquifer (SC/S-1, SC/S-12, SC/S-13). Group 2 includes four wells in the semi-confined/shallow aquifer (SC/S-2, SC/S-3, SC/S-5, SC/S-6) and two wells in the deep confined aquifer (DC-1, DC-17). All Group 2 monitoring points are located south of the resurgence belt, within the hydrogeological complex of the LP. The subdivision of Flow 2-Path 2 into Group 1 and Group 2 is based on the hydrogeological boundaries established in the pre-existing conceptual model of the study area (Di Renzo et al., 2024). Specifically, the groups are defined by their position relative to the resurgence belt and by the distinct lithological and hydraulic characteristics associated with the HP and LP aquifer systems. While this classification originates from the conceptual hydrogeological framework rather than statistical clustering, the seasonal dataset provides further support for this subdivision, as the two groups exhibit distinct and hydrogeologically coherent patterns in their geochemical and isotopic behaviour. To facilitate data interpretation, the seasonal behaviour of the two groups is described separately in the following sections.

4.2.2.1. Group 1. The seasonal variations observed along Path 2-Group 1 of Flow 2 in the main physicochemical parameters, major ions, stable water isotopic compositions, computed pCO_2, and calcite and dolomite saturation indices are reported in Table 5S. The basic statistics of the seasonal geochemical survey are presented in Table 2.

The results reveal distinct seasonal variations; in particular, the monitoring points belonging to this group exhibit seasonal variability of varying intensity in pH, EC, T, and the concentrations of the main ions, especially HCO_3^-, Mg^{2+}, Ca^{2+}, and NO_3^-. In detail, the pH values show a

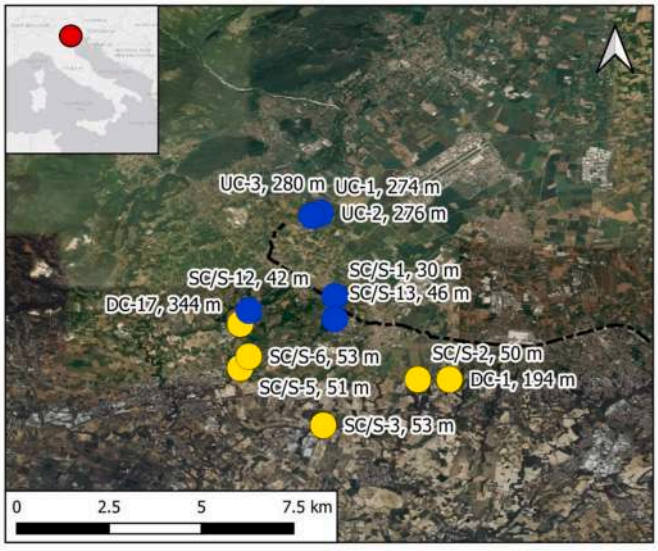


Fig. 5. Spatial subdivision of the monitoring points in Path 2 within Flow 2. Waters from Group 1 are represented in blue, while Group 2 waters are highlighted in yellow. (For interpretation of the references to colour in this figure legend, the reader is referred to the Web version of this article.)

median value of 7.80 for summer 2021, 7.58 for winter 2021, 7.68 for summer 2022, and 7.35 for winter 2022. T and EC show median values of 13.1 °C and 357 μS/cm for summer 2021, 11.4 °C and 280 μS/cm for winter 2021, 12.8 °C and 352 μS/cm for summer 2022, and 11.1 °C and 257 μS/cm for winter 2022, respectively. Regarding the seasonal trends of the major ions, the HCO_3^- and Ca^{2+} values show median concentrations of 205 mg/l and 46.3 mg/l in summer 2021, 195 mg/l and 43.9 mg/l in winter 2021, 210 mg/l and 48.6 mg/l in summer 2022, and 187 mg/l and 40.8 mg/l in winter 2022, respectively. The Mg^{2+} values show a median concentration of 19.1 mg/l in summer 2021, 17.4 mg/l in winter 2021, 20.3 mg/l in summer 2022, and 16.3 mg/l in winter 2022. The SO_4^{2-} and NO_3^- values show median concentrations of 4.0 mg/l and 6.9 mg/l in summer 2021, 4.0 mg/l and 6.7 mg/l in winter 2021, 4.5 mg/l and 8.0 mg/l in summer 2022, and 3.1 mg/l and 5.5 mg/l in winter 2022, respectively. Finally, Cl^-, Na^+ and K^+ do not exhibit pronounced seasonal variation. Overall, pH, EC, and T values, together with the concentrations of the main ions, tend to be higher during the summer period than during the winter period (Fig. 6a). This trend is likely attributable to the pronounced sensitivity of these waters to recharge inputs affecting the aquifers of the HP. The relationship between recharge events and seasonal variability is especially evident when examining the saturation indices of calcite and dolomite (Fig. 6b). Recharge events influence the groundwater's chemical equilibrium, thereby altering mineral saturation states (Wang et al., 2024). Accordingly, distinct seasonal patterns are observed, with the SI values clearly separating winter periods, characterized by a stronger recharge influence, from summer conditions. Specifically, $SI_{calcite}$ and $SI_{dolomite}$ values had medians of 0.22 and 0.31 during summer 2021; −0.06 and −0.22 in winter 2021; 0.24 and 0.42 in summer 2022; and −0.27 and −0.62 in winter 2022. These seasonal shifts are likely due to dilution effects associated with recharge inputs, which are consistent with observed seasonal variations in EC. This dilution may result from the mixing of recharge waters, generally more undersaturated with respect to carbonate minerals, with pre-existing groundwater that is closer to saturation, in accordance with the carbonate-rich geology of the region. This mechanism also contributes to explaining the observed decreases in HCO_3^-, Mg^{2+} and Ca^{2+} concentrations during winter months, as these solutes are influenced in carbonate environments, by calcite and dolomite dissolution-precipitation dynamics (Zhang et al., 2021). Further evidence of this relationship is highlighted by the seasonal trend of stable isotopes, particularly $\delta^{18}O$ (Fig. 6c). The isotopic values of $\delta^{18}O$ and $\delta^{2}H$ during the seasonal study show median values, respectively, of −8.24 and −55.3‰ in summer 2021; −8.02 and −54.8‰ in winter 2021; −8.36 and −55.4‰ in summer 2022; and −7.92 and −54.0‰ in winter 2022. It is important to note that seasonal variations of $\delta^{18}O$ did not show consistent responses in both monitoring years. Furthermore, these variations were observed to affect different water types differently. Specifically, for unconfined aquifers (UC-1, UC-2, UC-3), the variations depicted in Fig. 6c can be correlated with the fluctuations in the piezometric level of the aquifer located in the HP. An analysis of the piezometric level trends at the nearest station to the study area reveals that the observed $\delta^{18}O$ variations are temporally consistent with the piezometric fluctuations.

These findings highlight a co-variation between periods of higher and lower piezometric levels and the geochemical evolution of unconfined aquifers. On the other hand, semi-confined and shallow aquifers (SC/S-1, SC/S-12, SC/S-13) display seasonal variations that follow the seasonal piezometric level trend, but with a more attenuated response, indicating a marked influence of recharge during the winter period compared with the summer period. This moderated hydrological behaviour can likely be attributed to the lithological transitions occurring along the resurgence belt. The consistent co-variation observed between $\delta^{18}O$ values and piezometric levels supports the use of stable isotopes as tracers of recharge dynamics in unconfined aquifers, which are hydraulically connected to the surface and thus highly responsive to recharge from precipitation and surface water bodies (Matiatos and

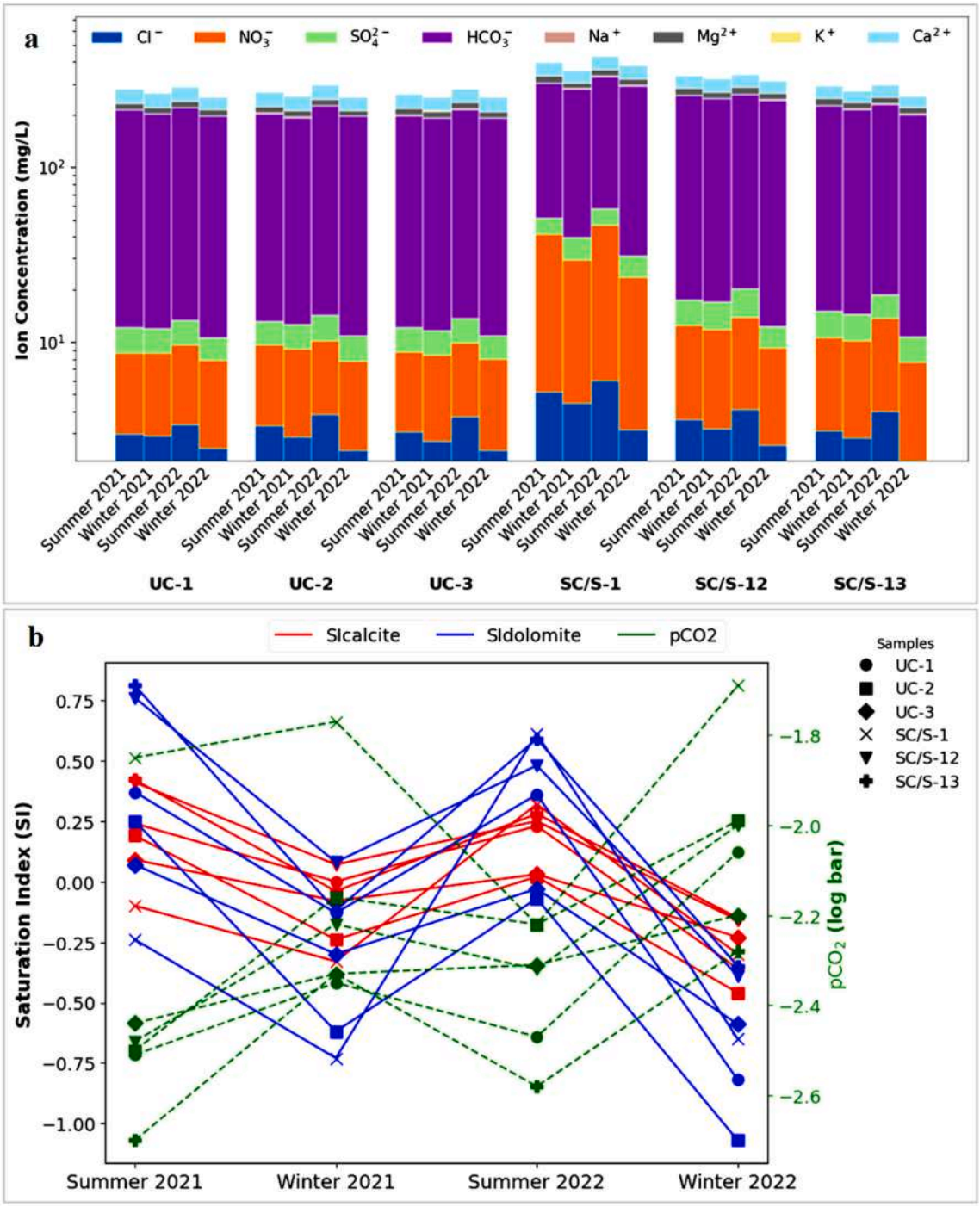


Fig. 6. The seasonal trends of the major ions (a), pCO_2 and saturation Index (SI) of calcite and dolomite (b), and $\delta^{18}O$ (c) for the Flow 2 – Path 2 – Group 1.

Wassenaar, 2019; Ansari et al., 2022). In this context, the observed isotopic response is consistent with the hydrogeological characteristics of the unconfined aquifer of the HP, which is primarily recharged through the gravel beds of rivers and by direct infiltration of meteoric water (Zini et al., 2009). The recharge system therefore reflects a complex, multi-source contribution from adjacent river systems, most notably the Cellina-Tagliamento Rivers and the western Cansiglio hydrographic basin, as highlighted by Cucchi et al. (2008), Zini et al. (2009), and Di Renzo et al. (2024).

Ultimately, these integrated tracers demonstrate that the baseline groundwater composition in this domain is governed by a dynamic interplay between multi-source recharge dilution and carbonate dissolution dynamics. Within this natural framework, while less pronounced than major ion shifts, pCO_2 exhibits a detectable pattern intrinsically linked to hydrological dynamics. Median values show a subtle but consistent increase during winter periods (−2.28 log bar in winter 2021; −2.03 log bar in winter 2022) compared to summer conditions (−2.49 log bar in summer 2021; −2.32 log bar in summer 2022). This winter elevation can be reasonably attributed to rising piezometric levels associated with recharge events, which act to flush biogenic CO_2 from the soil zone down into the aquifer. This mechanism explains the concurrent drop in calcite and dolomite saturation indices (SI) during

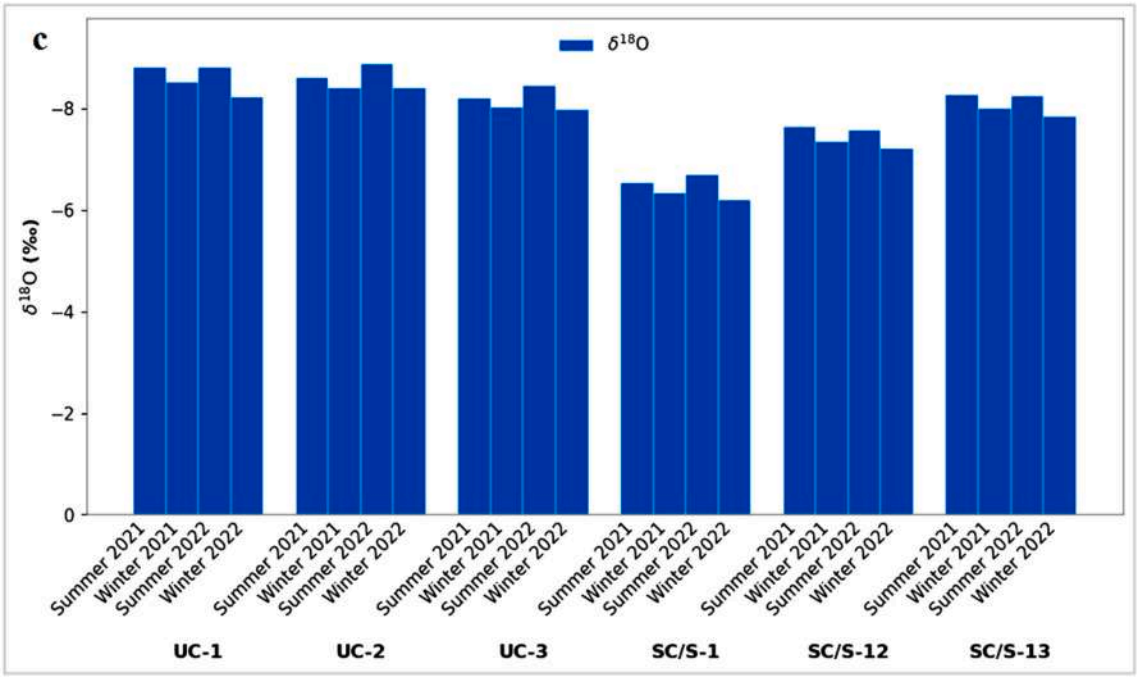


Fig. 6. (*continued*).

winter, as the influx of CO_2-rich recharge water temporarily increases the aggressiveness of the groundwater. This 'first flush' effect is particularly evident in winter 2022, likely reflecting a concentrated recharge pulse of soil-derived CO_2 following the preceding summer drought. The soil-derived origin of this dissolved inorganic carbon (DIC) is further constrained by $\delta^{13}C$ data from Zini et al. (2009), who reported for these aquifers a mean value of −8.08‰. This intermediate isotopic signature is characteristic of carbonate mineral dissolution driven by biogenic (soil-respired) CO_2, reflecting the expected isotopic mixing between marine carbonates ($\delta^{13}C \approx 0$‰) and soil-derived carbon ($\delta^{13}C \approx -25$‰).

In addition to these natural hydrogeological controls, the shallow groundwater system is also affected by anthropogenic inputs. Given their hydrogeological context and relatively shallow depths (30–40 m), the monitoring points are particularly susceptible to agricultural influences (Table 2S). In agreement with Cucchi et al. (2008), Zini et al. (2011), and Orecchia et al. (2022), the SC/S samples present the highest NO_3^- and SO_4^{2-} values within the group and, above all, a more pronounced seasonal variation, especially during the summer period when fertilization activities are taking place. During this period, summer rainfall events and field irrigation may facilitate the mobilisation of nitrate and sulphate toward the groundwater. This anthropogenic input temporarily modifies the Ca/Mg-HCO_3 hydrochemical facies, with an enrichment trend in NO_3^- and SO_4^{2-}, providing a potential seasonal indicator for distinguishing agricultural inputs from natural hydroclimatic variability (Fig. 5Sa). This process was described by Rotiroti et al. (2023), who identified how groundwater-fed irrigation promotes higher concentrations due to the recirculation of high-NO_3-SO_4^{2-} groundwater in the summer period when rainfall decreases and the demand for water for irrigation increases. The influence of agricultural activities appears to be less pronounced in the UC samples, likely because these waters are generally deeper and therefore less directly affected by surface-derived inputs. However, the pronounced summer increase in SO_4^{2-} concentrations cannot be attributed to agricultural inputs alone. Instead, our integrated analysis of stable isotopes and conservative tracers (d-excess and Cl^-) suggests that this summer geochemical shift is driven, probably, by a synergistic interplay of three co-occurring processes: lateral river recharge, agricultural mobilisation, and localized evapoconcentration (Ansari et al., 2023, 2025).

The relationship between $\delta^{18}O$ and d-excess provides further evidence of the different degrees of evaporation affecting the monitored groundwater (Fig. 5Sb). The UC samples generally show relatively depleted $\delta^{18}O$ values (approximately −8.9 to −8.0‰) associated with relatively high d-excess values (approximately 10–15‰), indicating limited modification by evaporation. A similar isotopic signature is observed in the deeper SC/S-13 well, which shows $\delta^{18}O$ values ranging from −8.27 to −7.86‰ and d-excess values between 9.18 and 11.68‰. In contrast, SC/S-12 exhibits an intermediate isotopic signature, with relatively enriched $\delta^{18}O$ values (−7.65 to −7.23‰) and lower d-excess values (3.78–5.80‰). The most pronounced deviation is observed in SC/S-1, where $\delta^{18}O$ values are markedly enriched (−6.70 to −6.20‰) and d-excess values are close to zero (−0.3–2.4‰). This combination of $\delta^{18}O$ enrichment and strongly reduced d-excess is consistent with evaporation affecting shallow groundwater and indicates that SC/S-1 is particularly susceptible to evaporative enrichment. The progressive shift from relatively depleted $\delta^{18}O$ and high d-excess values in the UC and deeper SC/S wells towards enriched $\delta^{18}O$ and low d-excess values in SC/S-1 therefore suggests a spatially heterogeneous influence of evaporation, which appears to be strongest in the shallowest portion of the resurgence belt.

This interpretation is further supported by the relationship between d-excess and Cl^- (Fig. 5Sc), which provides an additional indication of the concentration effects associated with evaporation. While the unconfined aquifers (UC-1 to UC-3) exhibit moderate d-excess values (10–15‰) and low, stable Cl^- (3 mg/L) indicative of relatively buffered subsurface mixing, well SC/S-1 displays a distinct evaporation-related signature. Screened at the shallowest depth (27.0–29.0 m) within the resurgence belt transition zone, SC/S-1 shows exceptionally low d-excess values (0.2–2.4‰), enriched $\delta^{18}O$ (−6.2 to −6.7‰), and elevated Cl^- (5 mg/L). These observations suggest that shallow water tables in this specific zone are highly susceptible to summer evapoconcentration, which may enhance the concentration of dissolved species, including sulphates. This evaporative concentration is superimposed on an aquifer baseline already potentially enriched in sulphates by the Tagliamento River. During dry summer months, the river may act as a losing stream, continuously infiltrating its distinct sulphate-calcic water (average $SO_4^{2-} \approx 141$ mg/L;) into the highly permeable, shallow gravel beds. Driven by the south-westward regional groundwater flow (Zini et al.,

2009), this riverine sulphate plume may therefore contribute to groundwater chemistry in the Pordenone Plain. Concurrently, summer irrigation may mobilise additional sulphate and nitrate from agricultural fertilizers. This seasonal river-to-aquifer recharge may become an important control on groundwater chemistry in the shallow aquifer, particularly in the absence of diluting rainfall (Cucchi et al., 2008; Zini et al., 2023). The role of depth in mitigating these surface-driven processes is further highlighted by the comparison between SC/S-1 and deeper semi-confined wells. For instance, well SC/S-13 (screened at 41.0–44.5 m) exhibits isotopic and chemical signatures (d-excess 9–12‰, low Cl^-) similar to those of the unconfined aquifers. This suggests that the evaporative and hydrochemical anomalies are largely confined to the shallowest zones of the resurgence belt, whereas deeper portions of the aquifer remain more effectively buffered.

Ultimately, the rapid seasonal resetting of the isotopic baseline across all wells supports a high degree of seasonal responsiveness and hydraulic connectivity within the plain aquifers. However, the distinct vulnerability of the shallowest zones highlights that sustainable management in intensively irrigated alluvial plains requires the effects of natural river-driven recharge, anthropogenic contamination, and climate-driven evapoconcentration to be distinguished and jointly considered (Ansari et al., 2023, 2025).

4.2.2.2. Group 2. The seasonal variations observed along Path 2-Group

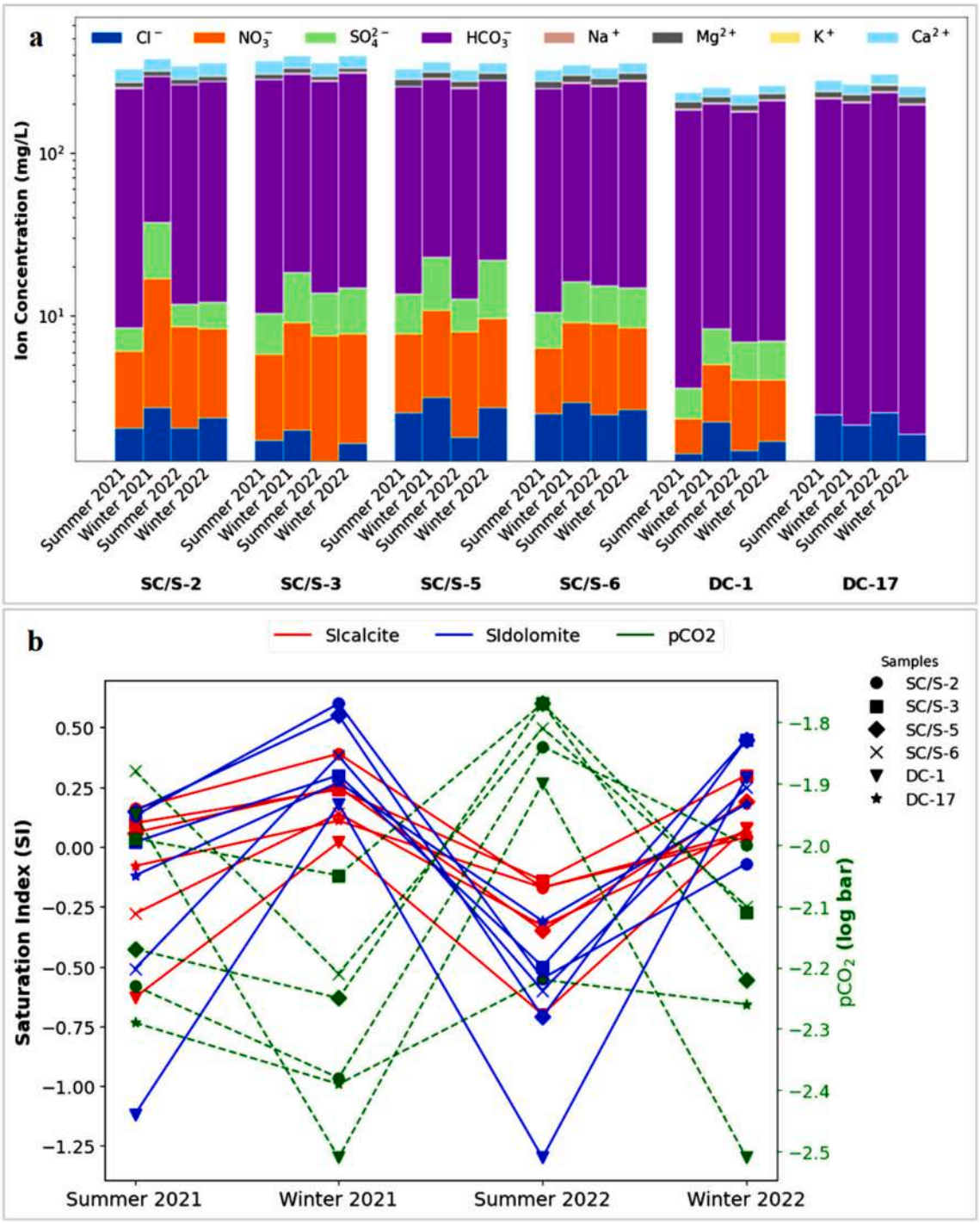


Fig. 7. The seasonal trends of the major ions (a), pCO_2 and saturation Index (SI) of calcite and dolomite (b), and $\delta^{18}O$ (c) for the Flow 2 – Path 2 – Group 2.

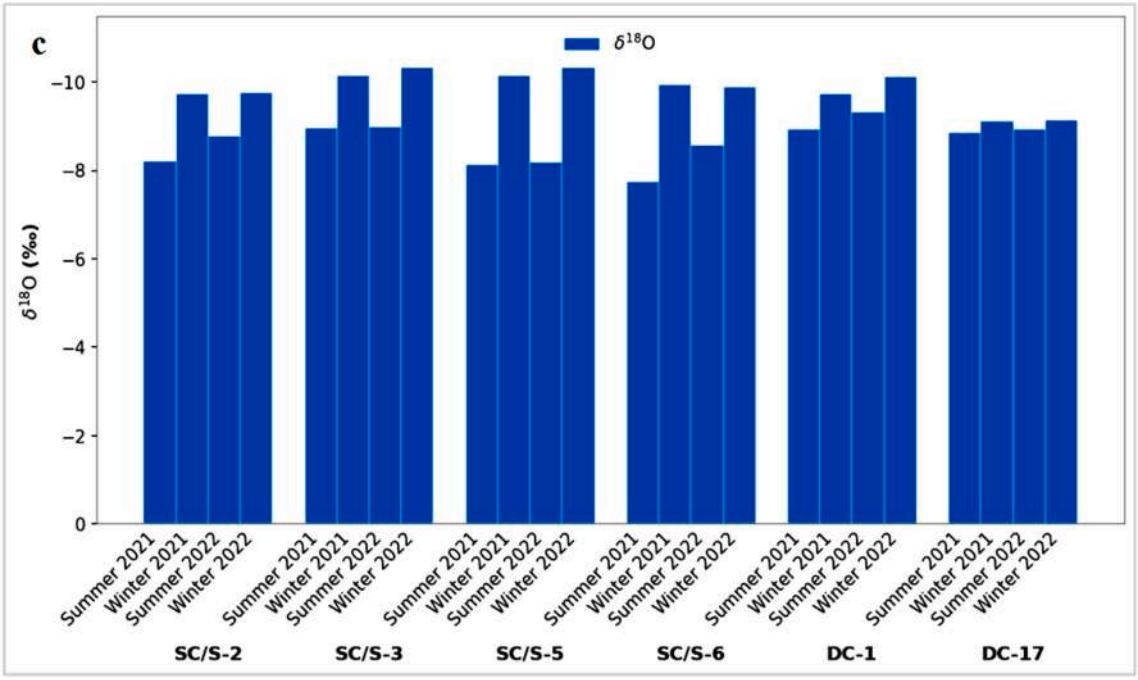


Fig. 7. (*continued*).

2 of Flow 2 in the main physicochemical parameters, major ions, stable water isotopic compositions, pCO_2 and calcite and dolomite saturation indices are reported in Table 5S. The descriptive statistics of the seasonal geochemical survey are presented in Table 3.

The results reveal distinct seasonal variations. As observed for Group 1, the monitoring points belonging to this group exhibit seasonal variability of varying intensity in pH, EC, T, and concentrations of the main ions, particularly HCO_3^-, Mg^{2+}, Ca^{2+}, and NO_3^-. In contrast to Group 1, however, pH, EC, T values, and the concentrations of the main ions generally show higher values during the winter period than during the summer period, in accordance with Orecchia et al. (2022). This inverse seasonal pattern is also evident in the major ion concentrations shown in Fig. 7a, which display marked and broadly consistent seasonal variability. In detail, the pH values show a median value of 7.50 for summer 2021, 7.65 for winter 2021, 7.20 for summer 2022, and 7.55 for winter 2022. The T and EC values show median values of 12.8 °C and 283 μS/cm for summer 2021; 13.5 °C and 356 μS/cm for winter 2021; 12.8 °C and 274 μS/cm for summer 2022; 13.9 °C and 344 μS/cm for winter 2022, respectively. Regarding the seasonal trends of the major ions, the HCO_3^- and Ca^{2+} values show median concentrations of 237 and 45.4 mg/l in summer 2021; 252 and 48.1 mg/l in winter 2021; 237 and 45.8 mg/l in summer 2022; and 257 and 48.1 mg/l in winter 2022, respectively. The Mg^{2+} values show median concentrations of 20.8 mg/l in summer 2021, 20.5 mg/l in winter 2021, 20.2 mg/l in summer 2022, and 21.3 mg/l in winter 2022. The SO_4^{2-} and NO_3^- values show median concentrations of 4.2 and 4.0 mg/l in summer 2021; 9.4 and 7.1 mg/l in winter 2021; 4.7 and 6.2 mg/l in summer 2022; and 6.4 and 6.0 mg/l in winter 2022, respectively. Finally, Cl^-, Na^+ and K^+ do not show marked seasonal variation. Overall, the winter period is characterised by higher pH, EC, T, and concentrations of the main ions than the summer period, indicating an inverse seasonal pattern compared with Group 1. This pattern is consistent with a delayed recharge response, whereby the effects of recharge reaching the LP aquifers are temporally decoupled from the seasonal forcing observed in the HP.

The seasonal increase in SO_4^{2-} and NO_3^- concentrations is particularly relevant for interpreting the hydrochemical evolution of these waters. Similar to the SC/S samples in Group 1, the Group 2 monitoring points are subject to anthropogenic influences, primarily from agricultural fertilisers. This anthropogenic input is reflected in the Ca/Mg–HCO_3 hydrochemical facies by a relative enrichment in NO_3^- and SO_4^{2-}, as highlighted by the modified Langelier–Ludwig diagram (Fig. 6Sa). This enrichment may provide a potential seasonal indicator for distinguishing agricultural inputs from natural hydroclimatic variability. However, the seasonal increase in SO_4^{2-} and NO_3^- concentrations alone does not fully explain the inverse seasonal pattern observed in the Group 2 waters.

The seasonal variation is also evident when considering the saturation indices of calcite and dolomite (Fig. 7b). The SI value for calcite and dolomite show a median, respectively, of 0.08 and 0.08 in summer 2021; 0.19 and 0.34 in winter 2021; −0.25 and −0.58 in summer 2022; 0.08 and 0.27 in winter 2022. The higher SI values generally observed during winter are consistent with the higher mineralisation of the groundwater during this period, whereas the lower values observed during summer are compatible with a greater influence of relatively dilute recharge. This summer drop in saturation indices is further supported by pCO_2 dynamics, which exhibit higher values during summer periods (−2.08 log bar in summer 2021; −1.83 log bar in summer 2022) compared to winter (−2.27 log bar in winter 2021; −2.17 log bar in winter 2022). This temporal shift in the pCO_2 peak, relative to the winter peak observed in Group 1, is consistent with the delayed recharge hypothesis. It suggests that the CO_2-rich recharge water infiltrating the High Plain during winter may take several months to cross the resurgence belt and reach the Low Plain aquifers in summer. The arrival of this CO_2-enriched water would temporarily increase groundwater aggressiveness, providing a coherent chemical explanation for the concurrent undersaturation with respect to carbonate minerals.

The stable isotope data provide further constraints on the origin and timing of the recharge signal (Fig. 7c). The isotopic values of $\delta^{18}O$ and δ^2H during the seasonal study show median values, respectively, of −8.56 and −58.5‰ in summer 2021; −9.83 and −64.1‰ in winter 2021; −8.88 and −59.5‰ in summer 2022; −9.99 and −64.4‰ in winter 2022. To further constrain the recharge processes and evaluate potential evaporation, mixing, and groundwater renewability in the LP aquifers, stable isotope data were integrated with conservative tracers (Cl^- and d-excess). The dataset reveals a distinct seasonal isotopic pattern consistent with delayed recharge mechanism (Fig. 6Sb). During

summer 2021, all semi-confined wells (SC/S-2 to SC/S-6) exhibit enriched $\delta^{18}O$ values (−7.73 to −8.98‰) coupled with low d-excess values (6.5–12.9‰), reflecting the delayed arrival of winter precipitation recharge from the previous hydrological year. Conversely, during winter 2021, these same wells display depleted $\delta^{18}O$ values (−9.71 to −10.3‰) and elevated d-excess values (13.6–19.1‰), consistent with the delayed arrival of the summer 2021 snowmelt signal that recharged the HP aquifers approximately six months earlier. A similar seasonal pattern is observed in 2022, although the isotopic shift is less pronounced. Overall, this inverse seasonal isotopic pattern provides evidence of a delayed recharge response within the LP aquifers.

Significantly, the relationship between d-excess and Cl^- (Fig. 6Sc) provides additional evidence that significant post-recharge evaporative enrichment is unlikely in the LP. Unlike the shallow wells near the resurgence belt in the HP (e.g., SC/S-1), which display low d-excess values (<3‰) and relatively elevated Cl^- concentrations, all LP wells exhibit low and stable Cl^- concentrations (1.3–3.2 mg/L) coupled with d-excess values that remain broadly consistent with meteoric recharge and show no clear evidence of evaporative depletion. These observations support the interpretation that the observed isotopic shifts primarily reflect the delayed arrival of meteoric recharge rather than significant modification by in-situ evaporation or mixing with evaporated surface water.

The processes hypothesized to govern the observed seasonal variations are consistent with those affecting the groundwater in Group 1. However, these waters exhibit an inverse seasonal trend, which may be attributed to the specific hydrogeological setting in which they occur. The samples belonging to this group share similarities with the SC/S-1, SC/S-12, and SC/S-13 in Group 1, which are semi-confined aquifers with an average depth of 40-50 m. The key distinction between the two groups lies in their geographical location, as the Group 2 monitoring points are located south of the resurgence belt, which acts as a hydrogeological transition zone characterized by a marked decrease in permeability. Indeed, Cucchi et al. (2008) highlight a transition in the FP from a transmissivity of approximately 10^{-2}-10^{-4} m^2/s in the phreatic aquifer of the HP (Mosetti, 1983; Carniel, 1999) to 10^{-7} m^2/s in the confined aquifers of the LP (Mosetti, 1983). Furthermore, based on the hydraulic conductivity values of the hydrogeological complexes defined by Cucchi et al. (2008), the aquifers of the HP, hosted in gravels and conglomerates, exhibit values of 10^{-2}-$7*10^{-3}$ m/s, whereas the aquifers of the LP, hosted in sands and peaty sands, show values of $2.5*10^{-4}$-$5*10^{-5}$ m/s. Within the proposed conceptual model, this marked reduction in permeability along the resurgence belt is inferred to decrease groundwater flow velocities. This hydrodynamic framework provides a consistent explanation for the "delayed seasonal recharge response" recorded in the LP compared with the HP (Cuthbert et al., 2019; Moeck et al., 2020), even though groundwater velocities and travel times were not directly measured in this study.

Within this framework, DC-17 represents a particular case within the deep confined aquifers of the LP. Despite its greater depth and reduced exposure to surface-derived inputs, this well shows a limited seasonal response in $\delta^{18}O$, suggesting that the delayed recharge signal may still reach the deeper portion of the aquifer. However, the relatively narrow ranges of d-excess (7.8–9.5‰), $\delta^{18}O$ (−8.84 to −9.12‰), and Cl^- concentrations (1.9–2.5 mg/L) indicate that this response is strongly attenuated compared with the shallower wells. In contrast, the other deep confined wells associated with Flow 3 show no appreciable seasonal variation. DC-17 may therefore represent an intermediate hydrogeological condition between the seasonally-responsive aquifers of Flow 2 and the more strongly buffered system associated with Flow 3.

Ultimately, documenting this inverse seasonal evolution of hydrochemical and isotopic parameters provides further evidence for refining existing conceptual models of heterogeneous alluvial plains (e.g., Cuthbert et al., 2019; Moeck et al., 2020). The results indicate that lithological transitions may not simply attenuate groundwater flow but can also contribute to a temporal decoupling of hydrochemical responses. This finding suggests that contamination monitoring in such environments should account for asynchronous responses between hydraulically connected but hydrogeologically distinct domains, which is relevant for developing resilient groundwater management strategies under increasing climate variability (Noble and Ansari, 2019; Kumar and Ansari, 2021).

Despite the delayed response, the seasonal variability of the isotopic baseline observed across the LP wells indicates their hydraulic responsiveness to surface-derived recharge. However, the approximately six-month lag introduces an important management implication: contamination events or recharge anomalies in the HP may not be immediately detectable in the LP, requiring monitoring strategies that account for this temporal decoupling.

4.3. Seasonal geochemical/isotopic characterization of flow 3

Based on the conceptual geochemical and isotopic model developed by Di Renzo et al. (2024), the deep confined aquifers of the LP are recharged by a deep flow system that is distinct from the other hydrogeological flows identified in the PP. This deep flow originates in the Alpine sector and is characterized by a gradual and slow outflow. The pronounced cation exchange process between the groundwater and the surrounding clay-rich sediments, together with the low tritium concentrations, are consistent with a slow flow system that is hydraulically isolated from the shallower groundwater systems of the PP. Regarding the seasonal variations along Flow 3, the monitoring data for water samples from the confined deep aquifers of the LP show no pronounced seasonal trends (Table 6S).

The descriptive statistics of the seasonal geochemical survey are presented in Table 4. In detail, the pH values show a median of 7.35 in summer 2021; 7.32 in winter 2021; 7.38 in summer 2022; and 7.35 in winter 2022. The T and EC values show a median, respectively, of 17.9 °C and 377 μS/cm in summer 2021; 17.2 °C and 350 μS/cm in winter 2021; 17.7 °C and 362 μS/cm in summer 2022; and 17.6 °C and 381 μS/cm in winter 2022. The temperature measurements therefore indicate a relatively stable thermal regime throughout the monitoring period, with values generally ranging from approximately 17 to 20 °C in the deeper wells. Rather than a distinct thermal anomaly, these relatively elevated temperatures are consistent with the expected geothermal gradient at these depths, as observed in several areas of northeastern Italy (Cucchi et al., 2008; Petrini et al., 2013; Cultrera et al., 2018; Pola et al., 2020; Torresan et al., 2022). Although this thermal regime represents an interesting hydrogeological characteristic, its potential for low-enthalpy geothermal exploitation cannot be assessed from the present dataset and would require dedicated investigations, including heat-flow and subsurface-temperature measurements.

Regarding the chemical and isotopic composition, including major ion concentrations, calcite and dolomite saturation indices, pCO_2 and $\delta^{18}O$ and $\delta^{2}H$ values, no distinct seasonal variations were found in these waters. In detail, the HCO_3^- and Ca^{2+} values show a median, respectively, of 330 and 41.4 mg/l in summer 2021; 325 and 40.3 mg/l in winter 2021; 330 and 40.0 mg/l in summer 2022; and 330 and 40.6 mg/l in winter 2022. The Mg^{2+} values show a median of 13.0 mg/l in summer 2021, 12.0 mg/l in winter 2021, 12.4 mg/l in summer 2022, and 12.2 mg/l in winter 2022. The Cl^-, Na^+ and K^+ values show a median, respectively, of 2.1, 50.7 and 5.1 mg/l in summer 2021; 2.2, 48.3, and 4.8 mg/l in winter 2021; 2.2, 47.6 and 5.0 mg/l in summer 2022; and 2.0, 48.8 and 4.9 mg/l in winter 2022. Finally, the concentrations of SO_4^{2-} and NO_3^- remain below their respective detection limits of 0.1 mg/L and 0.05 mg/L.

Unlike the shallow and intermediate systems, the hydrochemical facies of this deep flow exhibit remarkable temporal stability, with no discernible seasonal shifts. This persistent chemical signature confirms a long, isolated flow path dominated by prolonged water-rock interaction and complete shielding from short-term meteoric recharge pulses

(Ansari et al., 2022). Overall, the waters retain a consistent Ca/Mg–HCO_3 rich in Na + K hydrochemical signature, with no appreciable seasonal shift in major-ion concentrations (Fig. 7Sa). The SI of calcite and dolomite values show a median, respectively, of 0.09 and −0.02 in summer 2021; 0.01 and −0.23 in winter 2021; 0.00 and −0.14 in summer 2022; 0.01 and −0.26 in winter 2022. Similarly, pCO_2 exhibits noticeable stability, with median values tightly clustered between −1.88 and −1.77 log bar across all four campaigns. This negligible variation further confirms the isolation of this deep system from surface-derived biogenic CO_2 pulses. The isotopic values of $\delta^{18}O$ an $\delta^{2}H$ during the seasonal study show median values of −10.6 and −71.1‰ in summer 2021; −10.7 and −71.4‰ in winter 2021; −10.7 and −70.7‰ in summer 2022; −10.8 and −71.5‰ in winter 2022. The limited variability in both saturation indices, pCO_2, and stable isotope compositions further supports the absence of a pronounced seasonal response in Flow 3.

Considering the relationship between $\delta^{18}O$ and d-excess (Fig. 7Sb), the dataset reveals a high degree of isotopic stability across all monitoring campaigns, with inter-campaign variations in $\delta^{18}O$ consistently below 0.5‰ and d-excess variations below 2‰. For instance, well DC-2 exhibits $\delta^{18}O$ values ranging from −10.33 to −10.42‰ and d-excess values from 8.13 to 9.09‰ over the entire monitoring period, coupled with stable Cl^- concentrations (1.94-2.16 mg/L). This temporal stability is consistent with the absence of significant post-recharge evaporation and provides no evidence of significant post-recharge evaporative enrichment. The relationship between d-excess and Cl^- (Fig. 7Sc) further supports the absence of significant evaporative concentration in these deep aquifers. All confined wells exhibit low and stable Cl^- concentrations (1.3-2.6 mg/L), while d-excess values remain relatively stable across seasons. The absence of a systematic decrease in d-excess associated with increasing Cl^- concentrations provides no clear evidence of evaporative concentration or mixing with strongly evaporated surface waters. This isotopic stability, combined with the complete absence of anthropogenic markers (NO_3^- and SO_4^{2-} below detection limits), is consistent with limited influence from modern surface-derived input and support the hydraulic separation of these deep aquifers from the shallower groundwater systems.

Interestingly, the confined aquifers display two distinct isotopic populations based on d-excess values (Fig. 7Sb-c). The first population (DC-3, DC-4, DC-5, DC-9, DC-10, DC-13, DC-16, DC-21) exhibits elevated d-excess values (14–23‰) coupled with more depleted $\delta^{18}O$ (−10.6 to −12‰), consistent with recharge from relatively high-altitude areas and/or snowmelt-influenced recharge. The second population (DC-2, DC-6, DC-7, DC-8, DC-11, DC-12, DC-14, DC-15) displays lower d-excess values (8–13‰) with less depleted $\delta^{18}O$ (−9.9 to −11.5‰), suggesting a greater contribution from rainfall and/or lower-altitude recharge sources. This isotopic heterogeneity likely reflects differences in recharge areas and/or flow paths within the Alpine catchment. Importantly, both populations maintain their distinct signatures over time without seasonal modulation, indicating that these recharge signals are preserved during groundwater circulation and are not substantially modified by short-term seasonal inputs. The combined chemical and isotopic evidence therefore indicates that Flow 3 is characterised by a stable hydrogeochemical signature and limited seasonal responsiveness. However, the available data do not allow groundwater residence times to be quantified directly. The persistence of the isotopic signatures, together with the low tritium concentrations reported in the conceptual model of Di Renzo et al. (2024), is consistent with relatively long groundwater residence times and limited modern recharge, although dedicated age-tracer investigations would be required to distinguish between decadal, centennial, or older groundwater components.

Finally, the potential for vertical mixing or upward leakage between the deep Flow 3 and the shallower Flow 2 systems was explicitly evaluated. The distinct and non-overlapping isotopic signatures (e.g., stable, depleted $\delta^{18}O \approx -10.7$‰ in Flow 3 vs. seasonally variable, enriched $\delta^{18}O \approx -8.0$‰ to −8.5‰ in Flow 2) and hydrochemical profiles (e.g., absence of NO_3^-/SO_4^{2-} and elevated Na^+ in Flow 3 possibly due to cation exchange) provide strong evidence against significant mixing during the study period. This isotopic and geochemical decoupling confirms the hydraulic isolation of the deep aquifer from the active shallow cycle, with the sole minor exception of well DC-17, which exhibits transitional characteristics but remains largely protected from shallow anthropogenic inputs. These findings demonstrate that the confined deep aquifers of the LP are effectively decoupled from the active shallow hydrogeological cycle of the PP and remain effectively protected from modern sources of anthropogenic contamination, validating the use of isotopic baselines to distinguish deep, resilient systems from surface-driven pollution (Ansari et al., 2020, 2023). By demonstrating that their temporal stability is not merely a passive lack of variation but a critical diagnostic feature of resilience against surface-driven climate and anthropogenic stressors, this study advances the understanding of deep alluvial systems. However, this resilience comes at the cost of extremely low renewability, highlighting that these deep aquifers should be managed as strategic, non-renewable reserves rather than sustainable resources for ongoing extraction. Indeed, deep groundwater reserves worldwide are increasingly recognised as strategic resources requiring protection from anthropogenic pressures and long-term climate change impacts (Macfarlane, 1998; Akouvi et al., 2008; Currell et al., 2012; Ravenscroft et al., 2018; Noble and Ansari, 2019; Lapuyade et al., 2020; Qian et al., 2020; Kumar and Ansari, 2021; Abd-Elaty and Zelenakova, 2022; Gayen, 2022; Rouillard et al., 2022; Zhang et al., 2022; Adeyeye et al., 2023; Lipparini et al., 2023).

5. Conclusion

The study conducted in the Pordenone Plain (PP) demonstrates how detailed seasonal geochemical and isotopic monitoring, grounded in a pre-existing conceptual hydrogeochemical model, can improve our understanding of the complex processes governing groundwater dynamics under seasonal climatic variability. In this case, seasonal monitoring enabled the assessment of aquifer responses to climatic fluctuations during the study period, with particular emphasis on system behaviour under drought conditions. The investigation focused on both the intermediate flow system, representing the most complex and heterogeneous hydrological component of the PP, and the deeper flow system. In detail.

i) The karst system feeding the foothill springs exhibits a rapid and highly dynamic response to surface hydroclimatic signals. Isotopic data and carbonate saturation indices are consistent with seasonal shifts, distinguishing between winter rainfall-driven recharge and summer snowmelt contributions. Notably, $\delta^{18}O$ depletion was recorded in all three springs during summer 2021, likely reflecting the delayed contribution of spring snowmelt. This pattern was not observed during the severe drought of summer 2022, when reduced snow accumulation limited the snowmelt contribution. Conversely, winter samples showed isotopic enrichment consistent with rainfall-driven recharge, highlighting the high sensitivity of this system to seasonal and extreme hydroclimatic conditions.

ii) The shallow/intermediate groundwater systems traversing the plain exhibit a markedly contrasting seasonal response across the resurgence belt, which acts as a critical hydrogeological boundary. North of the resurgence belt (Group 1), unconfined and semi-confined aquifers display a clear co-variation between geochemical/isotopic signatures and piezometric levels, reflecting a direct and relatively rapid response to recharge inputs. In contrast, aquifers south of the resurgence belt (Group 2) exhibit a pronounced seasonal inversion. Although these samples share characteristics with the semi-confined aquifers of Group 1, their position south of the resurgence belt marks a critical hydrogeological transition. Within our conceptual framework, this permeability contrast is inferred to reduce groundwater flow

velocities, providing a consistent explanation for the 'delayed seasonal recharge effect' observed in the Low Plain relative to the High Plain.

iii) In marked contrast to the dynamic karst and shallow/intermediate systems, the deep groundwater system of the Low Plain appears to be effectively decoupled from shallow, seasonally influenced dynamics. Over the two-year monitoring period, its geochemical and isotopic compositions remained remarkably stable, showing no pronounced seasonal trends. The consistently elevated temperatures are interpreted as reflecting the regional geothermal gradient rather than a localized thermal anomaly. Furthermore, the absence of surface-derived contaminants (e.g., NO_3^- and SO_4^{2-}) supports the interpretation that this deep, low-transmissivity flow represents a well-protected and stable groundwater reservoir that is largely buffered against short-term hydroclimatic fluctuations.

In summary, this study provides new insights into the seasonal hydrogeochemical dynamics of a complex hydrogeological system such as the PP. The integrated geochemical and isotopic monitoring approach, supported by climatic and hydrogeological data, proves effective in elucidating aquifer responses to short-term hydroclimatic variability and anthropogenic pressures, particularly during the drought conditions observed in summer 2022. Specifically, the conceptual model successfully captures the distinct real-world behaviours of these tracers: $\delta^{18}O$ and d-excess effectively distinguish between snowmelt and rainfall recharge sources, while the integrated analysis of d-excess and Cl^- allows the identification of evaporative enrichment and mixing processes across different hydrogeological domains. Although the monitoring period does not capture long-term climatic trends, the results demonstrate the potential of the proposed methodology to detect changing recharge conditions and seasonal anomalies that are consistent with the hydrological impacts expected under future climate change scenarios. This approach enables the detection of seasonal fluctuations and a more accurate characterization of system responses, providing a robust hydrogeochemical baseline to inform integrated management strategies aimed at preventing water quality degradation and supporting sustainable groundwater allocation. When coupled with quantitative hydrological assessment, these findings can contribute to the development of more effective and resilient groundwater management strategies.

Beyond the local scale, this study highlights the broader applicability and potential international relevance of the proposed integrated monitoring approach. The Pordenone Plain represents a valuable natural laboratory for investigating complex and heterogeneous alluvial systems in which permeability contrasts create distinct hydrogeological domains. The methodological framework developed here to identify delayed recharge responses and decouple short-term hydroclimatic variability from anthropogenic pressures is not limited to this specific area. Rather it provides a methodological framework applicable to hydrogeologists and water managers seeking to assess groundwater sustainability and resilience in similar alluvial aquifers, particularly under the increasing frequency of extreme drought events. Although the Pordenone Plain is not classified as semi-arid, it experiences severe summer droughts that provide a useful analogue for hydroclimatic stress conditions affecting water-scarce regions. Looking forward, projected climate change scenarios for the region, characterized by a shift from snow-to rain-dominated recharge and an increased frequency of drought events, suggest that the natural high d-excess summer buffer observed in this study may become increasingly less pronounced. This could promote solute concentration and evaporative effects in shallow systems. Concurrently, intensified land use and agricultural expansion may exacerbate the shallow evapoconcentration and nutrient loading (NO_3^-, SO_4^{2-}) already identified along the resurgence belt.

This study demonstrates that sustainable groundwater management should adopt a differentiated approach: shallow aquifers require active seasonal monitoring and optimized agricultural practices to mitigate summer solute mobilization, whereas deep, hydrochemically stable aquifers should be protected as strategic, drought-resilient reserves. Furthermore, the use of seasonal isotopic baselines to distinguish drought-related variations from anthropogenic contamination could provide a useful diagnostic approach for water managers in arid and semi-arid regions, where distinguishing climate-driven changes from pollution is particularly important. Finally, several limitations of the study should be acknowledged, particularly regarding data density, temporal variability, and the inherent hydrogeological complexity of the system. The temporal resolution of this dataset (four campaigns over two years) was designed to capture seasonal extremes in both geochemical and isotopic signatures rather than high-frequency, event-scale variations or to provide absolute groundwater residence times in the absence of dedicated environmental age-dating tracers (e.g., ^{14}C, ^{3}H). Therefore, while the inferred hydrogeochemical processes are highly plausible and consistent with the proposed conceptual model, individual geochemical and isotopic shifts should not be interpreted as uniquely diagnostic of a single source or short-term process. Future studies employing higher-frequency sampling will be essential to further constrain these dynamics and validate these observations over longer timescales.

CRediT authorship contribution statement

Dino Di Renzo: Writing – original draft, Methodology, Investigation, Formal analysis, Data curation, Conceptualization. **Luca Pizzino:** Writing – review & editing, Visualization, Validation, Supervision. **Goran Vižintin:** Writing – review & editing, Visualization, Validation, Supervision. **Carmela Vaccaro:** Writing – review & editing, Visualization, Validation, Supervision, Resources, Project administration, Funding acquisition.

Funding

The research activities were carried out thanks to the funding of the doctoral scholarship provided by the University of Ferrara and thanks to the logistical support and contribution to analytical costs provided by LTA Livenza Tagliamento Acque through the Consorzio Futuro in Ricerca of Ferrara.

Declaration of competing interest

The authors declare that they have no known competing financial interests or personal relationships that could have appeared to influence the work reported in this paper.

Acknowledgements

This work is dedicated to the memory of Dr. Nieto Yàbar, whose invaluable contributions to sampling and field campaign organization greatly supported this study. We also express our gratitude to Enrico Marin and the entire team at Livenza Tagliamento Acque (LTA), Portogruaro (VE), for their invaluable assistance in planning and executing this research project, as well as during the sampling campaign.

Appendix A. Supplementary data

Supplementary data to this article can be found online at https://doi.org/10.1016/j.apgeochem.2026.107130.

Data availability

Data will be made available on request.

References

Abbott, M.D., Lini, A., Bierman, P.R., 2000. $\delta^{18}O$, δD and ^{3}H measurements constrain groundwater recharge patterns in an upland fractured bedrock aquifer, Vermont, USA. J. Hydrol. 228 (1–2), 101–112.

Abd-Elaty, I., Zelenakova, M., 2022. Saltwater intrusion management in shallow and deep coastal aquifers for high aridity regions. J. Hydrol.: Reg. Stud. 40, 101026.

Adeyeye, O.A., Xiao, C., Yawe, A.S., Zhang, Z., Yang, W., Nnanwuba, U.E., Liang, X., 2023. Temporal groundwater quality, health risks and source point management zonation of multi-aquifers in Jilin Qian'an, Northeastern China. Environ. Geochem. Health 1–26.

Akouvi, A., Dray, M., Violette, S., de Marsily, G., Zuppi, G.M., 2008. The sedimentary coastal basin of Togo: example of a multilayered aquifer still influenced by a palaeo-seawater intrusion. Hydrogeol. J. 16, 419–436.

Ansari, M.A., Noble, J., Deodhar, A., Saravana Kumar, U., 2020. Atmospheric factors controlling the stable isotopes (δ18O and δ2H) of the Indian summer monsoon precipitation in a drying region of Eastern India. J. Hydrol. 589, 125139. https://doi.org/10.1016/j.jhydrol.2020.124636.

Ansari, M.A., Noble, J., Deodhar, A., Saravana Kumar, U., 2022. Isotope hydrogeochemical models for assessing the hydrological processes in a part of the largest continental flood basalts province of India. Geosci. Front. 13 (1), 101336. https://doi.org/10.1016/j.gsf.2021.101336.

Ansari, M.A., Noble, J., Saravana Kumar, U., Deodhar, A., Akhtar, N., Singh, P., Raj, R., 2025. Assessing the groundwater recharge processes in intensively irrigated regions: an approach combining isotope hydrology and machine learning. Geosci. Front. 16, 102105. https://doi.org/10.1016/j.gsf.2025.102105.

Ansari, M.A., Saravana Kumar, U., Noble, J., Akhtar, N., Akhtar, M.A., Deodhar, A., 2023. Isotope hydrology tools in the assessment of arsenic contamination in groundwater: an overview. Chemosphere 340, 139898. https://doi.org/10.1016/j.chemosphere.2023.139898.

ARPA - OSMER, 2008. Atlante Climatico Del Friuli-Venezia Giulia: 1. Precipitazioni, p. 42 published online in. www.meteo.fvg.it.

ARPA FVG, 2012. Rapporto Sullo Stato Dell'Ambiente, 1° Capitolo (Cambiamenti Climatici), 3° Capitolo (Qualità Delle Acque Sotterranee).

ARPA FVG-OSMER, 2018. Studio Conoscitivo Dei Cambiamenti Climatici E Di Alcuni Loro Impatti in Friuli-Venezia Giulia. Report integrale.

ARPA FVG-OSMER, 2023. In meteo e il clima. In: Segnali Dal Clima in FVG, Cambiamenti – Impatti – Azioni. Report Integrale.

Balestra, V., Fiorucci, A., Vigna, B., 2022. Study of the trends of chemical–physical parameters in different karst aquifers: some examples from Italian alps. Water 14 (3), 441.

Barbieri, M., Boschetti, T., Petitta, M., Tallini, M., 2005. Stable isotope (^{2}H, ^{18}O and $^{87}Sr/^{86}Sr$) and hydrochemistry monitoring for groundwater hydrodynamics analysis in a karst aquifer (Gran Sasso, Central Italy). Appl. Geochem. 20 (2005), 2063–2081. https://doi.org/10.1016/j.apgeochem.2005.07.008.

Calligaris, C., Zini, L., Treu, F., Iervolino, D., Lippi, F., Cucchi, F., 2010. Water sustainability in the Friuli-Venezia Giulia Plain. In Proceedings Of: 85° Congresso Nazionale Della. società Geologica Italiana, pp. 157–158, 6-8 Settembre 2010, Pisa, Italia.

Cao, X., Wu, P., Zhou, S., Sun, J., Han, Z., 2018. Tracing the origin and geochemical processes of dissolved sulphate in a karst-dominated wetland catchment using stable isotope indicators. J. Hydrol. 562, 210–222.

Carniel, D., 1999. Idrodinamica Della Falda Freatica in Destra Tagliamento Dalla Stretta Di Pinzano Fino Alla Fascia Delle Risorgive (Hydrogeological Knowledge of Phreatic Aquifers Between Pinzano and the Resurgence Belt in the Tagliamento Valley). Unpublished M. Sc thesis, University of Trieste, p. 124.

Carulli, G., 2006. Carta geologica del Friuli-Venezia Giulia alla scala 1:150.000. Regione Autonoma Friuli-Venezia Giulia, Direzione Regionale Ambiente E Lavori Pubblici, Servizio Geologico Regionale, 1 Tav. Note Illustrative, p. 48.

Cavallin, A., 1979. Assetto strutturale del Massiccio Cansiglio – cavallo, Prealpi Carniche Occ. Atti del 2 Convegno di Studi sul Territorio della provincia di Pordenone 15–32. Piancavallo, Oct. 19-20, 1979.

Çelik, M., Çallı, S.S., Karakaş, Z.S., 2022. The role of mineralogical studies in delineating the recharge area and groundwater circulation of Susuz springs, Central Taurus Belt, Turkey. Hydrogeol. J. 30 (8), 2399–2415.

Ciampittiello, M., Marchetto, A., Boggero, A., 2024. Water resources management under climate change: a review. Sustainability 16, 3590. https://doi.org/10.3390/su16093590.

Colombo, J.C., Skorupka, C.N., Bilos, C., Tatone, L., Cappelletti, N., Carolina Migoya, M., Astoviza, M., Speranza, E., 2015. Seasonal and inter-annual variability of water quality in the Uruguay River, Argentina. Hydrol. Sci. J. 60 (6), 1155–1163.

Cucchi, F., Franceschini, G., Zini, L., 2008. Hydrogeochemical investigations and groundwater provinces of the Friuli Venezia Giulia Plain aquifers, northeastern Italy. Environmental Geology 55, 985–999.

Cucchi, F., Massari, G., Oberti, S., 1999. Fluttuazioni della falda freatica nell'Alta Pianura friulana. Gortania-Atti Mus. Friul. St. Nat. 21, 39–51, 1999.

Cultrera, M., Boaga, J., Di Sipio, E., Dalla Santa, G., De Seta, M., Galgaro, A., 2018. Modelling an induced thermal plume with data from electrical resistivity tomography and distributed temperature sensing: a case study in northeast Italy. Hydrogeol. J. 26 (3), 837–851.

Currell, M.J., Han, D., Chen, Z., Cartwright, I., 2012. Sustainability of groundwater usage in northern China: dependence on palaeowaters and effects on water quality, quantity and ecosystem health. Hydrol. Process. 26 (26), 4050–4066.

Cuthbert, M.O., Gleeson, T., Moosdorf, N., Befus, K.M., Schneider, A., Hartmann, J., Lehner, B., 2019. Global patterns and dynamics of climate–groundwater interactions. Nat. Clim. Change 9 (2), 137–141.

Dansgaard, W., 1964. Stable isotopes in precipitation. Tellus 16, 436–468. https://doi.org/10.3402/tellusa.v16i4.8993.

Dar, F.A., Perrin, J., Ahmed, S., Narayana, A.C., Riotte, J., 2015. Hydrogeochemical characteristics of Karst Aquifer from a semi-arid region of Southern India and impact of rainfall recharge on groundwater chemistry. Arabian J. Geosci. 8, 2739–2750.

De Filippi, F.M., Iacurto, S., Grelle, G., Sappa, G., 2021. Magnesium as environmental tracer for karst spring baseflow/overflow assessment—a case study of the pertuso karst spring (Latium region, Italy). Water 13 (1), 93.

Di Renzo, D., Marrocchino, E., Telloli, C., Cinti, D., Copia, L., Ortega, L., Tassinari, R., Vaccaro, C., 2024. Multidisciplinary hydrogeochemical and isotopic assessment of the Pordenone plain (Northeastern Italy) for water resources sustainability. Appl. Geochem. 175, 106161.

Di Renzo, D., Rizzo, A., Telloli, C., Salvi, S., Marrocchino, E., Nieto Yàrab, D., Vaccaro, C., 2023. Geochemical and isotopic tracers to define the aquifer's vulnerability: the case study of the alluvial multi-aquifer system of the Friulian plain. Environ. Monit. Assess. 195, 781. https://doi.org/10.1007/s10661-023-11359-7, 2023.

DiSGAM, 2006. Rilevamento dello stato dei corpi idrici sotterranei della Regione Friuli-Venezia Giulia. Convenzione tra L'Arpa FVG E Il Disgam Dell. 'Università degli Studi di Trieste.

Donnini, M., Melelli, L., Vetuschi, Zuccolini, Fiorucci, F., Cardellini, C., Frondini, F., 2026. ARETA (Alpine caRbon cyclE daTAset): a dataset on physical, chemical and isotopic data of Alpine groundwaters. Sci. Data 13, 734. https://doi.org/10.1038/s41597-025-06541-0.

Drever, J.I., 1997. The Geochemistry of Natural Waters: Surface and Groundwater Environments, third ed. Prentice Hall.

EEA, 2018. European Waters Assessment of Status and Pressure 2018, 2018. European Environmental Agency, Publications Office of the European Union, Luxembourg. EEA Report, 7/2018. https://www.eea.europa.eu/publications/state-of-water.

Egidio, E., De Luca, D.A., Lasagna, M., 2024. How groundwater temperature is affected by climate change: a systematic review. Heliyon 10 (6), e27762. https://doi.org/10.1016/j.heliyon.2024.e27762. ISSN 2405-8440 2024.

Filippini, M., Squarzoni, G., De Waele, J., Fiorucci, A., Vigna, B., Grillo, B., Riva, A., Rossetti, S., Zini, L., Casagrande, G., Stumpp, C., Gargini, A., 2018. Differentiated spring behavior under changing hydrological conditions in an alpine karst aquifer. J. Hydrol. 556, 572–584. https://doi.org/10.1016/j.jhydrol.2017.11.040. ISSN 0022-1694.

Florineth, D., Schluchter, C., 2000. Alpine evidence for atmospheric circulation patterns in Europe during the last glacial maximum. Quat Res 54, 295–308. Washington, DC.

Fontana, A., 2006. Evoluzione geomorfologica della bassa pianura friulana e sue relazioni con le dinamiche insediative antiche. Monografie Museo Friulano Storia Naturale 47, Udine. Inclusa la Carta Geomorfologica della Bassa Pianura Friulana alla scala 1, 288, 50.000.

Fontana, A., Mozzi, P., Bondesan, A., 2008. Alluvial megafans in the veneto-friuli plain: evidence of aggrading and erosive phases during late Pleistocene and Holocene. Quat. Int. 189, 71–89.

Gayen, A., 2022. Review on sustainable groundwater development and management strategies associated with the largest alluvial multi-aquifer systems of indo-gangetic basin in India. In: Applied Geomorphology and Contemporary Issues. Springer International Publishing, Cham, pp. 411–423.

Guo, Y., Li, P., He, X., Wang, L., 2022. Groundwater quality in and around a landfill in northwest China: characteristic pollutant identification, health risk assessment, and controlling factor analysis. Expo. Health 14 (4), 885–901.

He, H., Chen, Z., Liu, Z., Gao, Z., Hu, L., Lu, C., Shao, J., Li, Y., 2023. Geochemical features of fluid in xiaojiang fault zone, Southeastern Tibetan plateau: implications for fault activity. Appl. Geochem. 148, 105507.

Hem, J.D., 1989. Study and interpretation of chemical characteristics of natural waters. In: third ed. US Geological Survey Water Supply Paper 2254.

Hu, K., Chen, H., Nie, Y., Wang, K., 2015. Seasonal recharge and mean residence times of soil and epikarst water in a small karst catchment of southwest China. Sci. Rep. 5 (1), 10215.

IPCC, 2021. Climate change 2021: the physical science basis. Contribution of working group I to the sixth assessment report of the intergovernmental panel on climate change [Masson-Delmotte, V., P. Zhai, A. Jimenez Cisneros, B. E., Oki, T., arnell, N. W., Benito, G., cogley, J. G., doll, P., Jiang, T. and Mwakalila, S. S., 2014. Freshwater resources. In: Field, C.B., Barros, V.R., Dokken, D.J., Mach, K.J., Mastrandrea, M.D., Bilir, T.E., Chatterjee, M., Ebi, K.L., Estrada, Y.O., Genova, R.C., Gimma, B., Kissel, E. S., Levy, A.N., MacCracken, S., Mastrandrea, P.R., White, L.L. (Eds.), Climate Change 2014: Impacts, Adaptation and Vulnerability. Part A: Global and Sectoral Aspects. Contribution of Working Group II to the Fifth Assessment Report of the Intergovernmental Panel on Climate Change. Cambridge University Press, Cambridge, pp. 229–269.

Jasechko, S., Seybold, H., Perrone, D., Fan, Y., Shamsudduha, M., Taylor, R.G., Fallatah, O., Kirchner, J.W., 2024. Rapid groundwater decline and some cases of recovery in aquifers globally. Nature 625, 715–721. https://doi.org/10.1038/s41586-023-06879-8, 2024.

Jeelani, G., Kumar, U.S., Bhat, N.A., Sharma, S., Kumar, B., 2015. Variation of $\delta^{18}O$, δD and ^{3}H in karst springs of south Kashmir, western Himalayas (India). Hydrol. Process. 29 (4), 522–530.

Jiménez Cisneros, B.E., Oki, T., Arnell, N.W., Benito, G., Cogley, J.G., Döll, P., Jiang, T., Mwakalila, S.S., 2014. Freshwater resources. In: Field, C.B., Barros, V.R., Dokken, D. J., Mach, K.J., Mastrandrea, M.D., Bilir, T.E., Chatterjee, M., Ebi, K.L., Estrada, Y.O., Genova, R.C., Girma, B., Kissel, E.S., Levy, A.N., MacCracken, S., Mastrandrea, P.R., White, L.L. (Eds.), Climate Change 2014: Impacts,Adaptation, and Vulnerability. Part A: Global and Sectoral Aspects. Contribution of Working Group II to the Fifth

Assessment Report of the Intergovernmental Panel on Climate Change. Cambridge University Press, Cambridge, United Kingdom and New York, NY, USA, pp. 229–269.
Kanduč, T., Mori, N., Kocman, D., Stibilj, V., Grassa, F., 2012. Hydrogeochemistry of alpine springs from North Slovenia: insights from stable isotopes. Chem. Geol. 300–301, 40–54. https://doi.org/10.1016/j.chemgeo.2012.01.012. ISSN 0009-2541 2012.
Khudair, M.Y., Kamel, A.H., Sulaiman, S.O., Al-Ansari, N., 2022. Groundwater quality and sustainability evaluation for irrigation purposes: a case study in an Arid region, Iraq. Int. J. Sustain. Dev. Plann. 17 (2), 413–419.
Krueger, E., Rao, P.S.C., Borchardt, D., 2019. Quantifying urban water supply security under global change. Glob. Environ. Change 56, 66–74.
Kumar, U.S., Ansari, M.A., 2021. Environmental protection: managing fresh water resources. In: Encyclopedia of Nuclear Energy. Elsevier, pp. 465–484. https://doi.org/10.1016/B978-0-12-819725-7.00064-7.
Lapuyade, F., Saltel, M., de Grissac, B., 2020. Setting sustainable abstraction limits in confined aquifers: example from deep confined aquifers in the Bordeaux region, France. Sustainable Groundwater Management: a Comparative Analysis of French and Australian Policies and Implications to Other Countries, pp. 229–251.
Lipparini, L., Chiacchieri, D., Bencini, R., Aaron, Micallef, 2023. Extensive freshened groundwater resources emplaced during the Messinian sea-level drawdown in southern Sicily, Italy. Commun. Earth Environ. 4, 430. https://doi.org/10.1038/s43247-023-01077-w.
Liu, Z., Groves, C., Yuan, D., Meiman, J., Jiang, G., He, S., Li, Q., 2004. Hydrochemical variations during flood pulses in the south-west China peak cluster karst: impacts of $CaCO_3$–H_2O–CO_2 interactions. Hydrol. Process. 18 (13), 2423–2437.
Liu, Z., Li, Q., Sun, H., Wang, J., 2007. Seasonal, diurnal and storm-scale hydrochemical variations of typical epikarst springs in subtropical karst areas of SW China: soil CO_2 and dilution effects. J. Hydrol. 337 (1–2), 207–223.
Liu, Z., Yu, X., Jia, G., 2019. Water uptake by coniferous and broad-leaved forest in a rocky mountainous area of northern China. Agric. For. Meteorol. 265, 381–389.
Lucianetti, G., Penna, D., Mastrorillo, L., Mazza, R., 2020. The role of snowmelt on the spatio-temporal variability of spring recharge in a dolomitic mountain group, Italian alps. Water 12 (8), 2256.
Macfarlane, P.A., 1998. Is sustainability a viable concept in the management of confined aquifers in Kansas? BULLETIN-KANSAS GEOLOGICAL SURVEY 97–116.
Malík, P., Slaninka, I., Švasta, J., Michalko, J., 2015. Oxygen isotope composition snapshot of spring waters in a karstified plateau. Hydrogeological and Environmental Investigations in Karst Systems, pp. 237–244.
Mance, D., Hunjak, T., Lenac, D., Rubinić, J., Roller-Lutz, Z., 2014. Stable isotope analysis of the karst hydrological systems in the Bay of Kvarner (Croatia). Appl. Radiat. Isot. 90, 23–34.
Martelli, G., Granati, C., 2007. Valutazione della ricarica del sistema acquifero della Bassa Pianura Friulana. Giornale di Geologia Applicata 5, 89–114.
Martelli, G., Granati, C., 2010. A comprehensive hydrogeological view of the friuli alluvial plain by means of a multi-annual quantitative and qualitative research survey. Mem. Descr. Carta Geol. d'It. XC, 181–208 (2010) figg. 26, tabb. 3.
Martelli, G., Granati, C., Roda, C., 2007. Criteri per la realizzazione di una rete di monitoraggio quantitativo e sperimentazione. In: APAT - Progetto per Il Monitoraggio Degli Acquiferi Della Bassa Pianura Friulana in Provincia Di Udine. Mem, vol. 75. Descrittive Carta Geol. Italia.
Masiol, M., Battistel, M., D'Alberto, L., D'Amico, M., Mario, G., Marciano, R., Dreossi, G., Pozzobon, A., Stenni, B., 2026. Hydrogeochemical assessment and vulnerability analysis of mountain springs in a karstic water system in northeastern Italy. J. Hydrol. 679 (Part A), 136159. https://doi.org/10.1016/j.jhydrol.2026.136159. ISSN 2026 0022-1694.
Matiatos, I., Wassenaar, L.I., 2019. Stable isotope patterns reveal widespread rainy-period-biased recharge in phreatic aquifers across Greece. J. Hydrol. 568, 1081–1092. https://doi.org/10.1016/j.jhydrol.2018.11.053. ISSN 0022-1694.
Mekonnen, M., Hoekstra, A., 2016. Four billion people facing severe water scarcity. Sci. Adv. 2. https://doi.org/10.1126/sciadv.1500323 e1500323-e1500323.
Meneghel, M., Sauro, U., Baciga, M.L., Fileccia, A., Frigo, G., Toniello, V., Zampieri, D., 1986. Sorgenti carsiche e erosione chimica nelle Prealpi Venete (Karstic springs and chemical erosion in the area of Prealpi Venete). – studi Trentini di Scienze Naturali. Acta Geol. 62, 145–172.
Mercure, J.F., Paim, M.A., Bocquillon, P., Lindner, S., Salas, P., Martinelli, P., Berchin, I. I., de Andrade Guerra, J.B.S.O., Derani, C., de Albuquerque Junior, C.L., Riberio, J. M.P., Knobloch, F., Pollitt, H., Edwards, N.R., Holden, P.B., Foley, A., Schaphoff, S., Faraco, R.A., Viñuales, J.E., 2019. System complexity and policy integration challenges: the Brazilian energy-water-food nexus. Renew. Sustain. Energy Rev. 105, 230–243.
Moeck, C., Grech-Cumbo, N., Podgorski, J., Bretzler, A., Gurdak, J.J., Berg, M., Schirmer, M., 2020. A global-scale dataset of direct natural groundwater recharge rates: a review of variables, processes and relationships. Science of the total environment 717, 137042.
Mosetti, F., 1983. Sintesi sull'idrologia del Friuli-Venezia Giulia (Summary of the Friuli-Venezia Giulia hydrology). Quaderni Ente Tutela Pesca 6, 1–296.
Nannoni, A., Piccini, L., 2022. Mixed recharge and epikarst role in a complex metamorphic karst aquifer: the pollaccia system, Apuan Alps (Tuscany, Italy). Hydrology 9 (5), 83.
Naoura, J., El Kati, I., Benaabidate, L., 2021. Assessment of Ras El Ma Karst spring features by structural and functional approaches at the region of Taza, Morocco. Journal of Ecological Engineering 22 (9).
Naranjo-Fernández, N., Guardiola-Albert, C., Aguilera, H., Serrano-Hidalgo, C., Montero-González, E., 2020. Clustering groundwater level time series of the exploited Almonte-Marismas aquifer in Southwest Spain. Water 12 (4), 1063. https://doi.org/10.3390/w12041063.
Noble, J., Ansari, M.A., 2019. Isotope hydrology and geophysical techniques for reviving a part of the drought prone areas of vidarbha, Maharashtra, India. J. Hydrol. 570, 495–507. https://doi.org/10.1016/j.jhydrol.2019.01.020.
Obergfell, C., Bakker, M., Maas, K., 2019. Identification and explanation of a change in the groundwater regime using time series analysis. Groundwater 57 (6), 886–894.
Oki, T., Kanae, S., 2006. Global hydrological cycles and world water resources. Science 313, 1068–1072. https://doi.org/10.1126/science.1128845. New York, N.Y.
Orecchia, C., Giambastiani, B.M., Greggio, N., Campo, B., Dinelli, E., 2022. Geochemical characterization of groundwater in the confined and unconfined aquifers of the northern Italy. Applied Sciences 12 (15), 7944.
Orombelli, G., Ravazzi, C., 1996. The Late Glacial and Early Holocene: chronology and paleoclimate. Il Quaternario, Roma 9 (2), 439–444.
Palcsu, L., Gessert, A., Túri, M., Kovács, A., Futó, I., Orsovszki, J., Puskás-Preszner, A., Temovski, M., Koltai, G., 2021. Long-term time series of environmental tracers reveal recharge and discharge conditions in shallow karst aquifers in Hungary and Slovakia. J. Hydrol.: Reg. Stud. 36, 100858.
Parkhurst, D.L., Appelo, A.A.J., 2013. User's guide to PHREEQC (version 2) – a computer program for speciation, batch reaction, one dimensional transport and inverse geochemical modeling. USGS Water Res Inv Rep 99–4259, 312. https://doi.org/10.3133/wri994259.
Petrini, R., Italiano, F., Ponton, Slejko, F.F., Aviani, U., Zini, L., 2013. Geochemistry and isotope geochemistry of the monfalcone thermal waters (northern Italy): inference on the deep geothermal reservoir. Hydrogeol. J. 21, 1275–1287.
Pola, M., Cacace, M., Fabbri, P., Piccinini, L., Zampieri, D., Torresan, F., 2020. Fault control on a thermal anomaly: conceptual and numerical modeling of a low-temperature geothermal system in the Southern alps foreland basin (NE Italy). J. Geophys. Res. Solid Earth 125 (5), e2019JB017394.
Qian, H., Chen, J., Howard, K.W., 2020. Assessing groundwater pollution and potential remediation processes in a multi-layer aquifer system. Environmental Pollution 263, 114669.
Ravenscroft, P., McArthur, J.M., Rahman, M.S., 2018. Identifying multiple deep aquifers in the Bengal Basin: implications for resource management. Hydrol. Process. 32 (24), 3615–3632.
Rispal, N., Arfib, B., Audra, P., Henry, P., Viguier, B., Zappelli, A., Mocochain, L., Jagercikova, M., Vallet-Coulomb, C., Miche, H., Cadilhac, L., Sivelle, V., Delestre, O., 2026. Impact of seasonal snow on the recharge of a mountain karst aquifer under climate change: the Dévoluy case study (Southern Alps, France). Hydrol. Earth Syst. Sci. 30, 4699–4720. https://doi.org/10.5194/hess-30-4699-2026, 2026.
Rotiroti, M., Sacchi, E., Caschetto, M., Zanotti, C., Fumagalli, L., Biasibetti, M., Bonomi, T., Leoni, B., 2023. Groundwater and surface water nitrate pollution in an intensively irrigated system: sources, dynamics and adaptation to climate change. J. Hydrol., 129868
Rouillard, J., Neverre, N., Rinaudo, J.D., 2022. Initiating collective action for the management of deep confined aquifer systems: application of a participatory scenario approach in France. Hydrogeol. J. 30 (1), 21–36.
Schewe, J., Heinke, J., Gerten, D., Haddeland, I., Arnell, N., Clark, D., Dankers, R., Eisner, S., Fekete, B., Colón-González, F.J., Gosling, S., Kim, H., Liu, X., Masaki, Y., Portmann, F., Satoh, Y., Stacke, T., Tang, Q., Wada, Y., Kabat, P., 2014. Multimodel assessment of water scarcity under climate change. Proceedings of the National Academy of Sciences of the United States of America 111, 3245–3250. https://doi.org/10.1073/pnas.1222460110.
Setiawan, O., Sartohadi, J., Hadi, M.P., Mardiatno, D., 2019. Delineating spring recharge areas inferred from morphological, lithological, and hydrological datasets on Quaternary volcanic landscapes at the southern flank of Rinjani Volcano, Lombok Island, Indonesia. Acta Geophysica 67 (1), 177–190.
Sprenger, M., Carroll, R.W.H., Marchetti, D., Bern, C., Beria, H., Brown, W., Newman, A., Beutler, C., Williams, K.H., 2024. Stream water sourcing from high-elevation snowpack inferred from stable isotopes of water: a novel application of d-excess values. Hydrol. Earth Syst. Sci. 28, 1711–1723. https://doi.org/10.5194/hess-28-1711-2024.
Stefanini, S., 1978. La falda freatica nell'Alta Pianura friulana. Quaderni IRSA 34 (14), 343–360. Roma.
Stefanini, S., Cucchi, F., 1976. Gli acquiferi nel sottosuolo della provincia di Gorizia (The aquifers in the Gorizia province). Quaderni Isontini Ricerca Acque 28, 347–366.
Stefanini, S., Cucchi, F., 1977. Gli acquiferi nel sottosuolo della Provincia di Udine (Friuli-Venezia Giulia). QUADERNI IRSA 34 (6), 131–147.
Teatini, P., Comerlati, A., Carvalho, T., Gutz, A.-Z., Affatato, A., Baradello, L., Accaino, F., Nieto, D., Martelli, G., Granati, G., Paiero, G., 2015. Artificial recharge of the phreatic aquifer in the upper friuli plain, Italy, by a large infiltration basin. Environ. Earth Sci. 73, 2579–2593. https://doi.org/10.1007/s12665-014-3207-8, 2015.
Terasmaa, J., Retike, I., Vainu, M., Priede, A., Lode, E., Pajula, R., Koit, O., Tarros, S., Bikše, J., Popovs, K., 2020. Joint methodology for the identification and assessment of groundwater dependent terrestrial ecosystems in Estonia and Latvia. In: Abdelazim, M.N., Zelenakova, M., Kubiak-Wójcicka, K. (Eds.), Water Resources Quality and Management in Baltic Sea Countries. Springer Nature, Switzerland, pp. 253–275. https://doi.org/10.1007/978-3-030-39701-2.
Torresan, F., Piccinini, L., Cacace, M., Pola, M., Zampieri, D., Fabbri, P., 2022. Numerical modeling as a tool for evaluating the renewability of geothermal resources: the case study of the Euganean Geothermal System (NE Italy). Environ. Geochem. Health 44 (7), 2135–2162.
Vincenzi, V., Riva, A., Rossetti, S., 2011. Towards a better knowledge of cansiglio karst system (Italy): results of the first successful groundwater tracer test. Acta Carsologica 40 (1), 147–159.

Wang, F., Chen, H., Lian, J., Fu, Z., Nie, Y., 2020. Seasonal recharge of spring and stream waters in a karst catchment revealed by isotopic and hydrochemical analyses. J. Hydrol. 591, 125595.

Wang, P., Zhang, W., Zhu, Y., Liu, Y., Li, Y., Cao, S., Hao, Q., Liu, S., Kong, X., Han, Z., Li, B., 2024. Evolution of groundwater hydrochemical characteristics and formation mechanism during groundwater recharge: a case study in the Hutuo River alluvial–pluvial fan, North China Plain. Sci. Total Environ. 915, 170159. https://doi.org/10.1016/j.scitotenv.2024.170159. ISSN 0048-9697.

Witte, J.P.M., Zaadnoordijk, W.J., Buyse, J.J., 2019. Forensic hydrology reveals why groundwater tables in the province of Noord Brabant (the Netherlands) dropped more than expected. Water 11 (3), 478.

Zhang, C., Duan, Q., Yeh, P.J.F., Pan, Y., Gong, H., Moradkhani, H., Gong, W., Lei, X., Liao, W., Xu, L., Huang, Z., Zheng, L., Guo, X., 2021. Sub-regional groundwater storage recovery in North China Plain after the south-to-north water diversion project. J. Hydrol. 597, 126156.

Zhang, J., Chen, L., Hou, X., Li, J., Ren, X., Lin, M., Zhang, M., Wang, Y., Tian, Y., 2022. Effects of multi-factors on the spatiotemporal variations of deep confined groundwater in coal mining regions, North China. Sci. Total Environ. 823, 153741.

Zhao, M., Zeng, C., Liu, Z., Wang, S., 2010. Effect of different land use/land cover on karst hydrogeochemistry: a paired catchment study of Chenqi and Dengzhanhe, Puding, Guizhou, SW China. J. Hydrol. 388 (1–2), 121–130.

Zini, L., Calligaris, C., Treu, F., Iervolino, D., Lippi, F., 2011. Risorse Idriche Sotterranee Del Friuli-Venezia Giulia: Sostenibilità Dell'Attuale Indirizzo. Edizioni EUT, Trieste, p. 89, 9-788883-033148.

Zini, L., Calligaris, C., Treu, F., Zavagno, E., Iervolino, D., Lippi, F., 2013. AQUA mundi Groundwater sustainability in the Friuli Plain. AQUA mundi 4, 41–54. https://doi.org/10.4409/Am-058-13-0051.

Zini, L., Calligaris, C., Treu, F., Zavagno, E., Iervolino, D., Lippi, F., 2023. Groundwater sustainability in the Friuli Plain. Acque Sotterranee - Italian Journal of Groundwater 12 (3), 77–92. https://doi.org/10.7343/as-2023-713.

Zini, L., Cucchi, F., Franceschini, G., Treu, F., 2009. Caratteristiche idrologiche e geochimiche delle riserve acquifere sotterranee della Pianura del Friuli-Venezia Giulia. Gortania – atti Museo Friul. Di Storia Nat 30, 5–30.